Astronomy & Astrophysics

The VIMOS Ultra Deep Survey

The role of HI kinematics and HI column density on the escape of Lyα photons in star-forming galaxies at 2 < z < 4[★]

L. Guaita[1], M. Talia[2,12], L. Pentericci[1], A. Verhamme[6], P. Cassata[3], B. C. Lemaux[5], I. Orlitova[9], B. Ribeiro[4],
D. Schaerer[6], G. Zamorani[2], B. Garilli[7], V. Le Brun[4], O. Le Fèvre[4], D. Maccagni[7], L. A. M. Tasca[4], R. Thomas[3],
E. Vanzella[2], E. Zucca[2], R. Amorin[10,11], S. Bardelli[2], M. Castellano[1], A. Grazian[1], N.P. Hathi[4,8],
A. Koekemoer[8], and F. Marchi[1]

[1] INAF – Osservatorio Astronomico di Roma, via Frascati 33, 00040 Monteporzio (RM), Italy
   e-mail: lucia.guaita@oa-roma.inaf.it
[2] INAF – Osservatorio Astronomico di Bologna, via Gobetti 93/3, 40129 Bologna, Italy
[3] Instituto de Fisica y Astronomía, Facultad de Ciencias, Universidad de Valparaíso, Gran Bretaña 1111, Playa Ancha, Valparaíso, Chile
[4] Aix Marseille Université, CNRS, LAM (Laboratoire d'Astrophysique de Marseille) UMR 7326, 13388 Marseille, France
[5] Department of Physics, UC Davis, One Shields Avenue, Davis, CA 95616, USA
[6] Geneva Observatory, University of Geneva, 51 Ch. des Maillettes, 1290 Versoix, Switzerland
[7] INAF–IASF, via Bassini 15, 20133, Milano, Italy
[8] Space Telescope Science Institute, 3700 San Martin Drive, Baltimore, MD 21218, USA
[9] Astronomical Institute of the Czech Academy of Sciences, Boční II/1401, 140 00 Praha 4, Czech Republic
[10] Cavendish Laboratory, University of Cambridge, 19 J.J. Thomson Avenue, Cambridge CB3 0HE, UK
[11] Kavli Institute for Cosmology, University of Cambridge, Madingley Road, Cambridge, CB30HA, UK
[12] Dipartimento di Fisica e Astronomia, Universitá di Bologna, via Gobetti 93/2, 40129 Bologna, Italy

ABSTRACT

Aims. We wish to assess the role of kinematics and neutral hydrogen column density in the escape and distribution of Lyα photons.
Methods. We selected a sample of 76 Lyα emitting galaxies from the VIMOS Ultra Deep Survey (VUDS) at $2 \leq z \leq 4$. We estimated the velocity of the neutral gas flowing out of the interstellar medium as the velocity offset, Δv, between the systemic redshift (z_{sys}) and the center of low-ionization absorption line systems (LIS). To increase the S/N of VUDS spectra, we stacked subsamples defined based on median values of their photometric and spectroscopic properties. We measured the systemic redshift from the rest-frame UV spectroscopic data using the CIII]1908 nebular emission line, and we considered SiII1526 as the highest signal-to-noise LIS line. We calculated the Lyα peak shift with respect to the z_{sys}, the EW(Lyα), and the Lyα spatial extension, Ext(Lyα-C), from the in the 2D stacked spectra.
Results. The galaxies that are faint in the rest-frame UV continuum, strong in Lyα and CIII], with compact UV morphology, and localized in an underdense environment are characterized by outflow velocities of the order of a few hundreds of km s^{-1}. The subsamples with smaller Δv are characterized by larger Lyα peak shifts, larger Ext(Lyα-C), and smaller EW(Lyα). In general we find that EW(Lyα) anti-correlates with Ext(Lyα-C) and Lyα peak shift.
Conclusions. We interpret these trends using a radiative-transfer shell model. The model predicts that an HI gas with a column density larger than 10^{20} cm^{-2} is able to produce Lyα peak shifts larger than >300 km s^{-1}. An ISM with this value of N_{HI} would favour a large amount of scattering events, especially when the medium is static, so it can explain large values of Ext(Lyα-C) and small EW(Lyα). On the contrary, an ISM with a lower N_{HI}, but large velocity outflows would lead to a Lyα spatial profile peaked at the galaxy center (i.e. low values of Ext(Lyα-C)) and to a large EW(Lyα), as we see in our data. Our results and their interpretation via radiative-transfer models tell us that it is possible to use Lyα to study the properties of the HI gas. Also, the fact that Lyα emitters are characterized by large Δv could give hints about their stage of evolution in the sense that they could be experiencing short bursts of star formation that push strong outflows.

Key words. techniques: imaging spectroscopy – galaxies: star formation – ISM: kinematics and dynamics – scattering – galaxies: high-redshift

1. Introduction

The production of Lyα photons depends on the on-going star formation. However, the escape depends on a large variety of galaxy properties. It was shown by radiative transfer models, hydrodynamical simulations (Verhamme et al. 2006; Laursen et al. 2011; Orsi et al. 2012; Duval et al. 2014; Gronke & Dijkstra 2016), and observed in high- and low-redshift galaxies (Erb et al. 2014; Rivera-Thorsen et al. 2015; Henry et al. 2015; Trainor et al. 2015) that interstellar medium (ISM) dust is able to absorb Lyα photons and neutral hydrogen (HI) is able to scatter them. The

---

emerging Lyα line profile can present two peaks (Neufeld 1990; Dijkstra et al. 2006; Verhamme et al. 2006). The dominant red peak can be detected even in low-resolution spectra and its shift with respect to the systemic redshift is related to the neutral hydrogen column density (N_{HI}) and gas kinematics such as stellar outflows.

In medium- and high-resolution spectra, it is also possible to detect a blue peak. Radiative transfer models predict that, for simple geometries, the intensity of the blue peak and the separation between red and blue peaks are also connected with the HI column density (Verhamme et al. 2015) and dust content. Hashimoto et al. (2015) estimated the N_{HI} in a sample of $z \sim 2.2$ galaxies by comparing the Lyα profiles derived from the 1D spectra with the models described in Schaerer et al. (2011). For the Lyα emitting galaxies that showed a significant blue peak, these authors estimated N_{HI} lower than 10^{19} cm^{-2}. Also, they measured an average velocity offset of the red peak with respect to the systemic redshift of the order of 170 km s^{-1} and explained this value by N_{HI} as low as $10^{18.9}$ cm^{-2} (see also Verhamme et al. 2017). Shibuya et al. (2014a) investigated the role of the interstellar medium (ISM) HI kinematics on the escape of Lyα photons in a similar sample. They inferred the velocity of stellar outflows from the shift of the low-ionization absorption lines with respect to the systemic redshift (redshift of optical emission lines). They did not find any clear correlation between outflow velocity and Lyα equivalent width and proposed that low N_{HI} can make a galaxy appear as a strong Lyα emitter. However, it is difficult to disentangle the effect of kinematics and N_{HI} because a proper kinematics measurement implies a very good knowledge of the galaxy systemic redshift. In addition to this, complicated kinematics in the interstellar and also in the intergalactic medium can influence the Lyα photon emission. For instance, the data studied in Smit et al. (2017) are consistent with a picture in which outflows of different velocities can shape the Lyα emission line at different wavelengths starting from the main peak to the wings.

The propagation of Lyα photons in the circum-galactic medium is also related to the HI properties and its scattering capability. The total size of the Lyα emission was observed to be generally more extended than the rest-frame UV continuum (Steidel et al. 2011; Hayes et al. 2013; Momose et al. 2014; Guaita et al. 2015; Wisotzki et al. 2016). In a sample of local star-forming galaxies, Pardy et al. (2014) and Hayes et al. (2014) found that an HI gas characterized by $N_{HI} > 10^{20}$ cm^{-2} can efficiently scatter Lyα photons and produce the most extended Lyα emissions. They also showed that the Lyα equivalent width anti-correlates with the HI total mass.

Matsuda et al. (2012) proposed that the Lyα spatial extension strongly depends on environment. In fact, they found that the spatial extension of Lyα increases as their surface density increases and that the highest values are observed in proto-clusters (see also Steidel et al. 2011). Furthermore, Momose et al. (2016) studied the Lyα spatial extension as a function of physical properties. They found that the largest Lyα emission sizes are observed for the galaxies with the smallest Lyα equivalent width and brightest UV luminosity, which are possibly the most massive (see also Zheng et al. 2016).

In the past 10 yr, the physical properties of the Lyα emitting galaxies and in particular of the LAEs (Lyα emitting galaxies with $EW(\text{Ly}\alpha) > 20$ Å as defined for example in Gronwall et al. 2007) have been inferred from the spectral energy distribution analysis and from the multi-wavelength images and spectra. The LAEs tend to occupy the low-mass end of the star-forming galaxy mass distribution; they are compact in the rest-frame UV, characterized by low dust content, low metallicity, high specific star formation rates, and tend to be experiencing bursts of star formation (e.g. Finkelstein et al. 2011; Nakajima et al. 2012; Hashimoto et al. 2013; Shibuya et al. 2014b; Vargas et al. 2014; Hagen et al. 2014). However, Lyα in emission is also observed for galaxies with a moderate amount of dust (e.g. Kornei et al. 2010; Guaita et al. 2011; Hathi et al. 2016). Also, there is evidence that the largest equivalent width LAEs present high-ionization state and low oxygen abundances (Erb et al. 2010; Nakajima et al. 2013; Trainor et al. 2016; Nakajima et al. 2016; Amorín et al. 2017). In fact, high-ionization absorption, such as the CIV$\lambda\lambda$1548,1550 doublet, and strong nebular emission lines, such as the collisionally excited CIII$\lambda\lambda$1907, 1909 doublet, are detected in their spectra.

Stark et al. (2014) suggested a correlation between the equivalent width of CIII$\lambda\lambda$1907,1909 and Lyα. They studied a sample of 17 strongly lensed galaxies at $z \sim 2$ characterized by $EW(\text{CIII]}1908)$ up to 15 Å and $EW(\text{Ly}\alpha)$ up to 150 Å and found that they are characterized by low stellar masses, low metallicity, and specific star formation rates more than 10 times those of typical $z \sim 2$–3 UV-selected star-forming galaxies. More recently, similar results were found by Amorín et al. (2017, hereinafter A17) for a sample of 10 low-mass galaxies at $z \sim 3$, selected by their strong Lyα ($EW(\text{Ly}\alpha) > 45$ Å) in the VIMOS Ultra-Deep Survey (Le Fèvre et al. 2015). While their properties closely resemble those typically found in galaxies at higher redshift ($z > 6$; e.g. Smit et al. 2014; Stark et al. 2017), the above studies suggest that low-mass galaxies showing strong CIII] and Lyα emission might be experiencing a vigorous phase of rapid galaxy growth (e.g. Gawiser et al. 2007). However, other studies just show correlations with some scatter (e.g. Rigby et al. 2015). The model described in Jaskot & Ravindranath (2016), for example, shows a weak trend between the equivalent widths of CIII] and Lyα. The scatter between these two quantities depends on the ionization parameter and metallicity of the starburst regions.

Using rest-frame UV spectroscopy of galaxies with both Lyα and CIII] in emission, we may focus on extreme cases of Lyα emission, but we can set the systemic redshift just looking at the same spectrum. Knowing the systemic redshift allows us to derive information on the kinematics of the ISM, obtained from low-ionization absorption lines, which trace the HI gas. Therefore, we can disentangle the effect of kinematics and HI column density on the shape of the Lyα emission line and its spatial extension.

With a large sample of Lyα+CIII] emitters from the VIMOS Ultra-Deep Survey (VUDS[1]; Le Fèvre et al. 2015; Tasca et al. 2017), we aim to study and characterize the spatial versus spectral escape of the Lyα emission from galaxies to investigate further if scattering is the main powering mechanism of the extended Lyα emission around galaxies. To do this, we present the Lyα equivalent width, the shape of the Lyα emission line, and the Lyα spatial extension in stacked spectra.

The paper is organized as follows. In Sect. 2 we present the spectroscopic data used in this analysis; in Sect. 3 we describe the method used to estimate the systemic redshift, generate stacked spectra, and measure kinematics features; in Sects. 4 and 5 we show and discuss our results. We summarize our work in Sect. 7. Throughout the paper, we use AB magnitudes and air wavelengths, the equivalent widths are expressed in the rest-frame system, and we adopt a standard cosmology.

---

[1] http://cesam.lam.fr/vuds/

2. Spectroscopic data

The spectra of the galaxies we analyse in this work are part of the VUDS, which is a deep spectroscopic survey of ~10 000 star-forming galaxies (SFGs) performed with the VISible MultiObject Spectrograph (VIMOS) instrument at the Very Large Telescope. The survey was designed to provide a complete census of high-redshift galaxies with the scope of studying the history of the global star formation, the build up of the mass function, and very young objects among many others. The VIMOS spectra are obtained with the LRBLUE and LRRED-grism settings in low-resolution mode ($R \sim 300$). The survey covers three extragalactic fields: the COSMOS field, the extended *Chandra* Deep Field South (ECDF-S), and the VVDS-02h field. Each spectrum is the result of 14 hours of integration in a wavelength range between ~4000 and ~9500 Å, which allows the study of SFGs at $2 \le z \le 7$, and is calibrated to air wavelength (for reference λ_{vacuum} ([CIII]) = 1907.71 Å and λ_{air} ([CIII]) = 1907.07 Å). Among the SFGs, we focused on the Lyα emitting galaxies ($EW(Ly\alpha) > 0$ Å, based on the EW measurements from Cassata et al. 2015) with reliable redshift (flags 3, 4, corresponding to a probability greater than 95% for the redshift to be correct) at $2 \le z \le 4$.

We excluded the sources detected in the most recent Xray surveys, which are thought to be active galactic nuclei (AGNs). For the COSMOS field, we cross-matched the VUDS Lyα emitting galaxies with the catalogue presented in Civano et al. (2016). We also double checked any possible Xray emission considering the catalogues by Civano et al. (2012), Kim et al. (2007), and Kalfountzou et al. (2014). For ECDF-S, we considered the X-ray catalogues from Xue et al. (2011) and from the 3XMM_DR4 survey[2]. We also removed from our sample the sources from the AGN lists by Fiore et al. (2012) and by Xue et al. (2011). For the VVDS-02h field, we excluded any source found in the XMDS/VVDS 4σ (Chiappetti et al. 2005) and in the 3XMM_DR4 survey catalogues.

The wavelength range of the spectra at $2 \le z \le 4$ includes Lyα, low-ionization interstellar absorption line systems (LIS), such as SiII1260, CII1334, SiII1526, and spectral features that trace the systemic redshift (z_{sys}). The LIS lines are produced in the ISM by the absorption of the stellar UV radiation and trace the kinematics of the HI gas (e.g. Talia et al. 2012). The photospheric stellar absorption lines, such as OIV1343, SiIII1417, and SV1500 (e.g. Talia et al. 2012), are the most commonly used systemic-redshift sensitive features. However, these lines tend to be very weak and do not reach enough signal to noise (S/N) to provide the z_{sys} of our individual spectra. Nebular emission lines, such as the CIII$\lambda\lambda$1907, 1909 doublet, are produced around massive stars in HII regions and can also trace the z_{sys}. Talia et al. (in prep.) showed concordance between z_{sys} obtained using stellar photospheric lines and that obtained from CIII] for the star-forming galaxies in VUDS.

In the individual spectra of the galaxies in our sample, the CIII doublet is blended and we refer to it as CIII]1908 (Stark et al. 2014). Even if we are limited by the low resolution, the CIII]1908 emission line provides the most reliable systemic redshift when its (integrated flux) S/N is larger than 3. We excluded the cases in which CIII] is blended to any OH line or is close to any artificial defect, which are situations that increase the noise locally (see Sect. 3.1).

Starting from 1070 Lyα emitting galaxies at $2 < z < 4$, we kept 79 showing S/N(CIII]1908) > 3. We then excluded three

sources with UV-line ratios consistent with an AGN ionization. We measured CIV1550/CIII]1908, CIV1550/HeII1640 and we referred to Fig. A.2 in Feltre et al. (2016) for the exclusion. This figure shows CIV1550/HeII1640 versus CIV1550/CIII]1908 and highlights the values of those ratios typical of star-forming galaxies and AGN. Finally, we compiled a sample of 76 galaxies. Among these galaxies, about two-thirds are characterized by Lyα equivalent width (EW) larger than 20 Å, the value commonly used to define Lyα emitters (LAEs).

In Fig. 1, we show the distributions of the properties of the 76 galaxies and of the initial 1070 sources. Our sample is not biased with respect to the initial sample in terms of physical properties, such as rest-frame UV magnitude, concentration, and redshift, except for $EW(Ly\alpha)$ and stellar mass. The median $EW(Ly\alpha)$ value of our sample is significantly larger than that of the 1070 sources. This is not surprising since we are selecting Lyα emitting galaxies that are also CIII] emitters with S/N(CIII]1908) > 3 and since earlier studies found, in general, a correlation between the CIII] and Lyα equivalent widths (Stark et al. 2014).

We considered the physical parameters obtained with the Le Phare SED fitting code (Arnouts et al. 1999), which was applied to the VUDS data as outlined in Tasca et al. (2017). By starting from the best available multiwavelength photometry and fixing VUDS spectroscopic redshift, they applied seven different Bruzual & Charlot (2003) models to obtain the best-fit stellar mass, star formation rate (SFR), age, and dust reddening. The models encompass star formation histories characterized by an exponentially decaying mode and delayed exponentially decaying modes. A Chabrier (2003) initial mass function is used and nebular emission lines are added to the stellar templates (Ilbert et al. 2009). The Lyα+CIII] emitters of our sample are characterized by stellar masses of $\log(M_*/M_\odot) = [8.4\text{--}10.9]$ with a median value of $\log(M_*/M_\odot) = 9.5$, dust reddening $E(B-V) = [0.0\text{--}0.3]$ with a median value of 0.1, and (uncorrected) SFR = 4–200 $M_\odot$ yr^{-1}, with a median value of 20 $M_\odot$ yr^{-1}.

In Fig. 2 we show stellar mass surface density, star formation rate surface density, and concentration versus stellar mass for the 1070 sources and for our 76 Lyα+CIII] emitters. The median stellar mass of our sample is 30% smaller than that of the initial sample and it is not characterized by extreme values of SFR and star formation rate surface density. Compared with the stellar mass surface density versus stellar mass of all the galaxies in VUDS (Ribeiro et al. 2016, Figs. 2 and 19), our sample occupies the low-mass end.

To summarize, our sample is composed of galaxies that tend to be faint and moderately concentrated in the rest-frame UV continuum. These galaxies are characterized by median rest-frame $EW(Ly\alpha) = 27$ Å, $EW(CIII]1908 = 7.9$ Å, and a median stellar mass of 2.9×10^9 $M_\odot$ (Fig. 1 and Table 1).

3. Method

Since the escape and the large-scale propagation of Lyα photons depend on the ISM kinematics, we wish to estimate kinematics features and its dependency with Lyα equivalent width, Lyα line shape, and Lyα spatial extension.

We first measured the systemic redshift of each Lyα+CIII] emitting galaxy (Sect. 3.1) and we defined six pairs of subsamples (listed in Table 1 and described in Sect. 3.2), based on physical and spectral properties, i.e. rest-frame UV magnitude, Lyα and CIII]1908 equivalent width, rest-frame UV concentration,
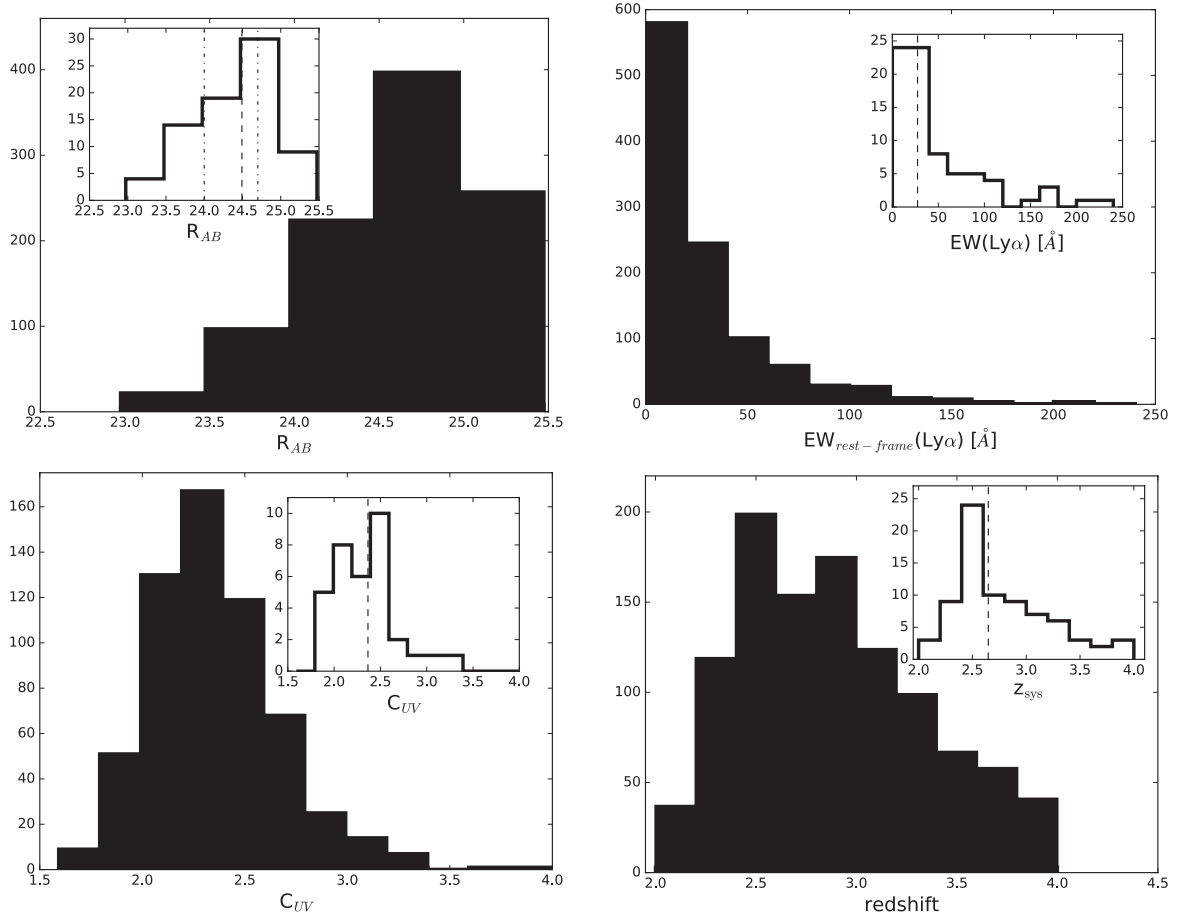
---

[2] http://xmmssc-www.star.le.ac.uk/Catalogue/3XMM-DR4/

Fig. 1. Distribution of *R* magnitude (*top left*), *EW*(Lyα) (*top right*), rest-frame UV concentration (*bottom left*), redshift (*bottom right*) of our sample of 76 sources (empty histograms in the *inserts*). Filled histograms correspond to the distributions of the 1070 Lyα emitting galaxies at $2 < z < 4$. The vertical dashed lines indicate the median value of each histogram. In the *top left panel*, the dot-dashed vertical lines indicate the median *R* values of the two bins obtained, separating the sample with respect to the median of the 76-galaxy distribution.
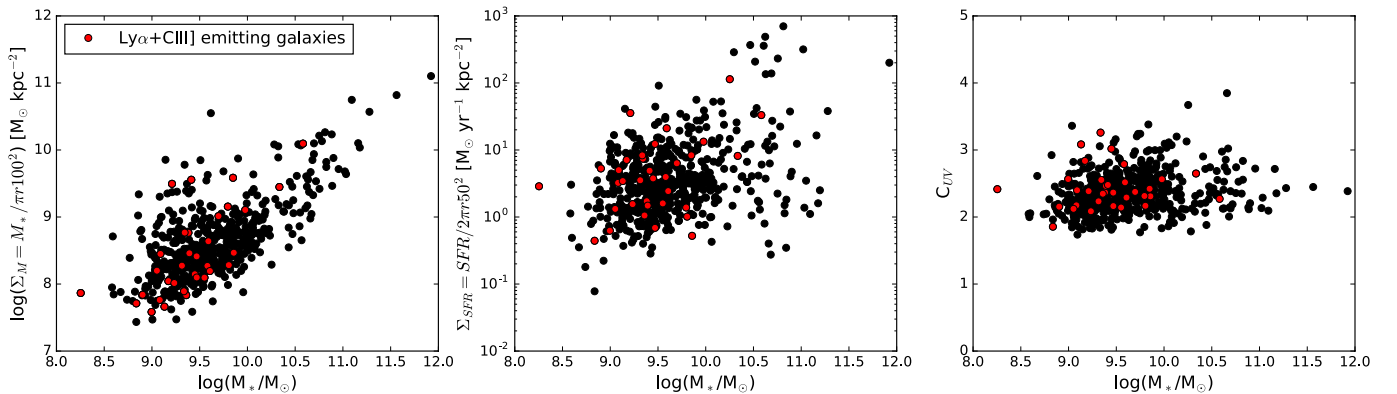

Fig. 2. Stellar mass surface density (*left*), star formation rate surface density (*middle*), and rest-frame UV concentration (*right*) as a function of stellar mass. To calculate the stellar mass surface density, we used the total-light radius, r100, while to calculate the star formation rate surface density, we used the half-light radius, r50, according to the definitions in Ribeiro et al. (2016). The size measurements can be performed for a limited number of sources for which the HST coverage is available. Black dots represent the Lyα emitting galaxies at $2 < z < 4$, while red dots correspond to those with S/N(CIII]1908) > 3.

environment density, and stellar mass; we stacked these pairs to increase the S/N of the individual spectra (Sect. 3.3). Then, we considered the LIS lines that trace the neutral gas to infer the HI kinematics (such as the velocity of stellar inflows/outflows). We quantified the kinematics by evaluating the offset between the systemic redshift and the central wavelength of the highest signal-to-noise LIS (Sect. 3.4).

3.1. Systemic redshift

The rest-frame UV continuum of the Lyα emitting galaxies in our sample is faint with a median *R* magnitude of 24.5. Stellar photospheric absorption lines, which are intrinsically weak features, have a S/N that is too low and cannot be recognized in individual spectra. Therefore, we estimated the systemic redshift (z_{sys}) from the CIII]1908 (Fig. 3). To estimate z_{sys}, we
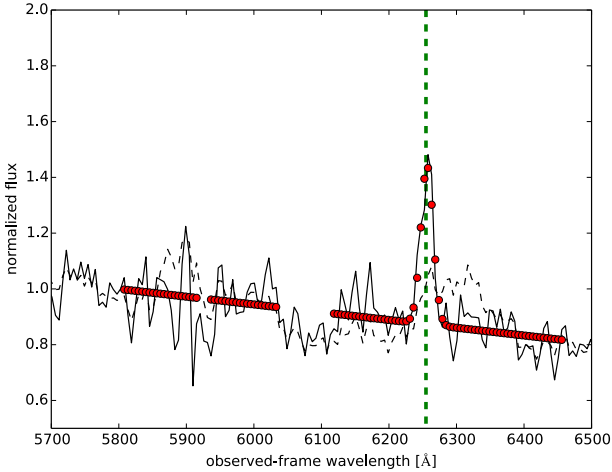
Fig. 3. Region of the spectrum covering the CIII]1908 emission line and the continuum around it for the source #510838687. The air observed-frame (noise) spectrum is presented as a solid (dashed) line. It is normalized to the continuum value. The vertical green line indicates the (air) wavelength of CIII] at VUDS redshift.

started with the VUDS redshift as a guess, and we fit together the CIII]1908 emission line and the continuum around it. We used the *optimize.leastsq* python function (as applied also in Guaita et al. 2013) by assuming a Gaussian profile, that the continuum has a well-defined slope (linear fit), and including the VUDS noise spectrum in the minimization procedure. This noise contains the information of the observation and the instrumental uncertainty. In fitting the continuum, we excluded the wavelength regions occupied by absorption lines that could alter the slope. We derived the galaxy systemic redshift from the best-fit mean of the Gaussian profile.

3.2. Definition of the sub-samples

From the VUDS spectra, we can compute three complementary Lyα quantities: the equivalent width $EW(Ly\alpha)$, the Lyα peak shift compared to systemic redshift, and the spatial extension of the Lyα line in the direction perpendicular to the slit (see the definitions below). The last two quantities are not measurable with enough accuracy on individual spectra, but on stacks only, as described later. In order to investigate which physical parameter, if any, drives the escape of Lyα radiation from galaxies, we computed several physical quantities for our galaxies. Then, we separated the sample of 76 galaxies in halves, according to the median values of R magnitude (representing the rest-frame UV at $2 < z < 4$), $EW(Ly\alpha)$, $EW(CIII]1908)$, and stellar mass as shown in Table 1.

The equivalent widths of CIII]1908 are consistent with the values typical of metal-poor galaxies (A17). The equivalent widths of Lyα and CIII]1908 were calculated in the 1D spectra from the flux integrated within the Gaussian fits of the lines and the fitted level of the local continua. From our total sample of 76 sources, 34 are located in the fields with HST coverage (Koekemoer et al. 2007, 2011; Grogin et al. 2011); we consider the rest-frame UV light concentration, C_{UV}, measure in Ribeiro et al. (2016) (equations 6, 7, 18, and 21). We generated two subsets, separating the 34 galaxies in halves according to the median C_{UV} value (2.4).

A Monte Carlo Voronoi tessellation technique was applied to the VUDS fields to estimate local (number) densities of galaxies (Lemaux et al. 2016, and Lemaux et al., in prep., where the technique is adapted for VUDS). We defined the delineation point for overdense and underdense regions as being the median density of a sample of VUDS galaxies in the redshift range $2 < z < 4$ matched in stellar mass to the Lyα emitting galaxy sample presented in this study. According to this density definition, we found that 26 out of 76 Lyα emitting galaxies are located in underdense and 50 in overdense regions. We generated the stacks of the 26 and 50 sources as shown in Table 1.

3.3. Stacking procedure

To generate the stacked 1D spectra, we normalized each observed-frame spectrum to the value of its continuum at 1650–1850 Å, a wavelength region free of strong absorption lines (Talia et al. 2012), and we obtained the rest-frame spectra using their z_{sys}. We took the median of the systemic redshifts within each subsample as the representative of the subsample stack. The range in z_{sys} within each subsample produces a range in wavelength steps of less than 0.5 Å in the rest frame (Fig. 1). Therefore, we resample each spectrum to a wavelength step of

$$step_\lambda = \frac{5.355}{1 + median(z_{sys})}, \tag{1}$$

where 5.355 is the nominal VIMOS_LR Å/pixel scale (of the observed-frame spectra) and $median(z_{sys})$ is the median z_{sys} of a certain subsample. Then, we stack the normalized rest-frame spectra by performing an average combination. The whole spectrum of each subset is presented in Appendix A. The noise of the stacked spectrum is created from the square root of the sum of the squares of the VUDS noise spectra of the N sources in a subsample,

$$noise_{stack} = \frac{\sqrt{\left(\sum_i^N (noise_i^2)\right)}}{N}. \tag{2}$$

In Figs. A.1 and A.2, we show the stacked 1D spectra of each subsample and we indicate emission and absorption features with vertical lines. The blue dashed, red dashed, and green solid lines indicate Lyα, HeII, and CIII], respectively. The black dashed lines indicate LIS and the dashed yellow stellar absorption lines. The stellar features are within the continuum noise. Instead, the Lyα and CIII]1908 emission lines and a few ISM absorption lines present enough S/N (larger than 3) to be identified with certainty. The equivalent widths of the absorption lines in the stacked spectra are also estimated from the ratio between the fluxes integrated within the Gaussian-fit curves and the linearly fitted continuum levels.

We also analysed the shape of the Lyα emission line in the stacked 1D and 2D spectra. Lyα peaks redward of z_{sys} and we estimated the corresponding velocity shift (Lyα peak shift) by fitting a Gaussian curve to the Lyα emission line in the 1D spectrum and by taking the best-fit center of the Gaussian (Fig. 4).

To estimate the errors on the Lyα peak shift, we applied the bootstrap technique. We adopted this technique because the uncertainties are calculated directly from the spectra as they are, without the need of choosing an arbitrary method to perturb the spectrum fluxes, as the usual Monte Carlo technique would require. Also, it is a random sampling technique that is able to deal with small samples. Following the bootstrap prescription, for the stacked spectrum of each subsample we generated 100 fake stacks, each one constructed from a group of galaxies drawn with a replacement from the subsample that was used for the real stack. On the fake stacks, we performed the same measurements

Table 1. Characteristics of the sub-sample stacks

Sub-sample property	N	$z_{\rm sys\,median}$	$R_{\rm median}$ AB	$SFR_{\rm median}$ $M_\odot$ yr^{-1}	$\Sigma_{SFR\,\rm median}$ $M_\odot$ yr^{-1} kpc^{-2}	$M_{*\,\rm median}$ 1E+9 $M_\odot$	Δv(SiII) km s^{-1}	EW(SiII) Å	EW(CIII]) Å	EW(Lyα) Å	Ext(Lyα–C) kpc	Lyα peak shift km s^{-1}
(1)	(2)	(3)	(4)	(5)	(6)	(7)	(8)	(9)	(10)	(11)	(12)	(13)
$R \geq 24.5$	38	2.9	24.7 ± 0.1	11.0 ± 3.3	4.4 ± 1.1	2.8 ± 2.4	−280 ± 100	−1.6 ± 0.5	13.3 ± 1.8	58.4 ± 9.0	5.3 ± 0.6	173 ± 62
$R < 24.5$	38	2.5	24.0 ± 0.1	28.8 ± 8.6	2.8 ± 1.7	3.1 ± 2.5	−20 ± 80	−0.9 ± 0.3	6.2 ± 0.9	22.7 ± 3.8	6.0 ± 0.6	428 ± 110
EW(Lyα) ≥ 27 Å	38	2.7	24.6 ± 0.1	14.0 ± 4.6	4.5 ± 1.5	3.1 ± 3.1	−360 ± 130	−1.2 ± 0.4	11.8 ± 2.2	71.3 ± 10.0	5.3 ± 0.4	196 ± 60
EW(Lyα) < 27 Å	38	2.6	24.3 ± 0.1	19.5 ± 8.7	2.9 ± 0.5	2.8 ± 1.6	−30 ± 60	−1.6 ± 0.6	7.6 ± 1.0	9.7 ± 1.3	6.4 ± 0.6	510 ± 98
EW(CIII]) ≥ 7.9 Å	38	2.9	24.7 ± 0.1	12.7 ± 8.3	4.1 ± 1.1	3.0 ± 3.3	−430 ± 180	−1.2 ± 0.7	15.2 ± 2.0	58.2 ± 11.6	4.8 ± 0.5	207 ± 80
EW(CIII]) < 7.9 Å	38	2.5	24.2 ± 0.1	20.1 ± 5.6	3.3 ± 1.6	2.7 ± 0.8	−30 ± 50	−1.8 ± 0.3	4.6 ± 0.2	22.0 ± 4.3	6.3 ± 0.5	307 ± 58
$C_{\rm UV} \geq 2.4$	17	2.7	24.7 ± 0.1	11.7 ± 3.4	4.1 ± 1.2	2.9 ± 2.1	−470 ± 200	−2.1 ± 1.3	13.3 ± 3.6	94.2 ± 18.3	4.7 ± 0.9	93 ± 72
$C_{\rm UV} < 2.4$	17	2.7	24.5 ± 0.1	20.5 ± 4.0	3.0 ± 1.5	2.9 ± 2.4	−80 ± 120	−2.0 ± 0.5	9.1 ± 1.8	16.0 ± 4.2	4.1 ± 1.4	325 ± 140
Over	50	2.7	24.5 ± 0.1	17.5 ± 4.9	3.7 ± 1.4	3.2 ± 1.8	−70 ± 60	−1.1 ± 0.3	8.8 ± 1.0	32.3 ± 5.8	5.7 ± 0.5	284 ± 76
Under	26	2.6	24.4 ± 0.1	17.6 ± 11.2	3.5 ± 0.6	2.7 ± 3.7	−400 ± 170	−1.8 ± 0.8	11.5 ± 3.0	58.4 ± 13.8	5.0 ± 0.8	160 ± 85
$M_* \geq$ 2.9E+9 $M_\odot$	38	3.0	24.3 ± 0.1	21.9 ± 9.0	4.3 ± 1.6	5.9 ± 3.1	−270 ± 120	−1.2 ± 0.3	11.0 ± 2.0	38.7 ± 9.5	5.0 ± 0.6	137 ± 59
$M_* <$ 2.9E+9 $M_\odot$	38	2.6	24.5 ± 0.1	14.7 ± 3.3	3.1 ± 0.9	1.9 ± 0.2	−63 ± 110	−1.4 ± 0.5	8.0 ± 0.8	41.0 ± 7.6	5.8 ± 0.5	322 ± 69

Notes. The columns correspond to: (1) the properties that define the sub-samples: R magnitude, Lyα and CIII]1909 equivalent widths, rest-frame UV concentration, field density, and stellar mass of the galaxies in our sample; (2) the number of sources in each sub-sample. Some of the sources in the sub-samples selected based on different properties overlap. The concentration is estimated only when we have HST coverage; for the sources in each sub-sample we report (3) the median systemic redshift; (4) the median R-band magnitude; (5) the median star-formation rate, obtained from the SED fitting; (6) the median star formation rate density calculated from the SFR and from the PSF-corrected half-light-radius measured in the HST I broad-band images (Σ_{SFR} =SFR/2 π r$^2_{1/2}$); and (7) the median stellar mass also obtained from the SED fitting. We report the error bars on the median values. It is up to 0.1 for R, of the order of 5 for SFR, 0.5–1.7 for Σ_{SFR}, 0.2–3.7 for M_*. Then, we show six quantities calculated in the stacks of the sub-samples: (8) the velocity offset between CIII] and SiII1526; (9) the rest-frame equivalent width of the SiII1526 absorption line; (10) the rest-frame equivalent width of CIII]1908; (11) the rest-frame equivalent width of Lyα; (12) the 2D Lyα spatial extension; (13) the Lyα peak shift.

as in the real stack. We estimated the Gaussian-fit parameters in each fake realization and calculated the standard deviation among the 100 realizations.

We explored the possibility of fitting the Lyα emission line with more sophisticated curves, such as a skewed Gaussian function with the following form:

$$f(\lambda) = Ne^{-(\lambda-\overline{\lambda})/2\sigma^2} \times \left[1 + erf((\lambda - \overline{\lambda})A)\right], \quad (3)$$

where A is the skewed parameter. However, given the low resolution of our spectra, the best-fit parameters obtained with this skewed Gaussian function are consistent with those obtained with a normal Gaussian fit. An example is shown in Fig. 4. We can see that symmetric and asymmetric curve fits produce consistent parameters within the bootstrap errors. Therefore, we perform our analysis of the 1D Lyα profiles with the simplest approach (i.e. the Gaussian fit).

To evaluate the spatial extension of the Lyα emission in each subsample, we first obtained the rest-frame 2D spectra and we aligned them in the spatial direction (Cassata et al., in prep.). We then averaged the aligned 2D spectra via the IRAF task *imcombine*. The Lyα spatial extension is estimated by fitting a Gaussian curve to the spatial profiles of Lyα and UV continuum around 1500 Å (Fig. 5). We obtain the full width half maximum (FWHM) of the Gaussian best fits (*FWHM*(Lyα) and *FWHM*(Cont)). We define the Lyα spatial extension with respect to the continuum as

$$Ext(Ly\alpha - C) = \sqrt{FWHM(Ly\alpha)^2 - FWHM(Cont)^2}. \quad (4)$$

When *FWHM*(Lyα) > *FWHM*(Cont), the Lyα spatial profile is more extended than the rest-frame UV continuum and Ext(Lyα-C) is defined. We adopt this definition to implicitly consider the deconvolution with the point spread function (PSF) of the observations, which is difficult to quantify in the stacked spectrum. In fact, a subtraction in quadrature of the PSF FWHM from FWHM(Lyα) and FWHM(Cont) cancels out in our formula[3].

Fig. 4. Flux density (f_λ) normalized to the area below the curves of the Lyα (black dots) emission line. We present the 1D-stack line of the subsample of the galaxies with EW(Lyα) ≥ 27 Å on *the top* and with EW(Lyα) < 27 Å on *the bottom panel*. In *the left panels*, we show the symmetric (red) and asymmetric (green) Gaussian best fits. In the *right panels*, we show the best fits of the 100 realizations of the same line generated to calculate the bootstrap uncertainties. For the EW(Lyα) ≥ 27 Å subsample, the Lyα peak shift from the symmetric (asymmetric) Gaussian fit is 196 ± 60 km s^{-1} (163 ± 63 km s^{-1}). For the EW(Lyα) < 27 Å subsample, it is 510 ± 98 km s^{-1} (516 ± 114 km s^{-1}) for the symmetric (asymmetric) Gaussian fit.

---

[3] The Ext(Lyα-C) we measure could be a lower limit of the true Lyα spatial extension. In fact, VUDS spectra are corrected for slit losses based on contin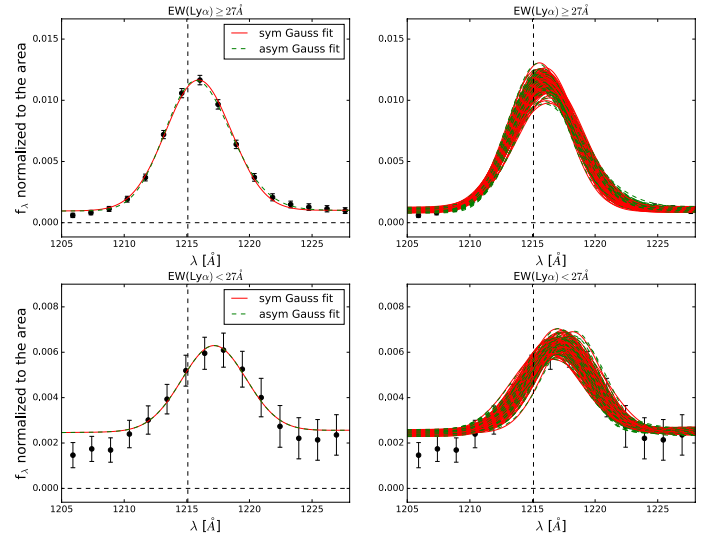uum magnitudes (Le Fèvre et al. 2015), but additional losses could affect Lyα if its emission is significantly more extended than the continuum (e.g. Huang et al. 2016). For instance, Lyα emission elongated perpendicularly to the spatial direction will be strongly affected by slit losses. Since we are considering stacks it is reasonable that severe losses will be compensated.
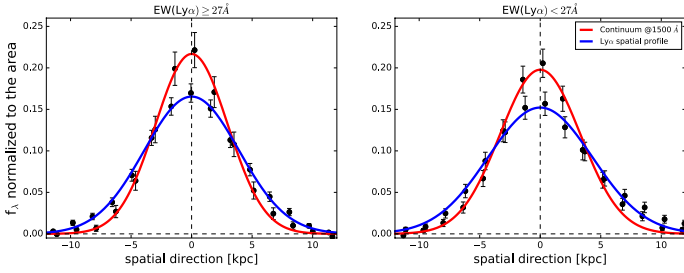
Fig. 5. Flux density (f_λ) normalized to the area below the curves of the Lyα (black dots and blue curve) and UV continuum (black dots and red curve) spatial profiles. We present the 2D-stack profiles of the subsample of the galaxies with $EW(Ly\alpha) \geq 27$ Å on the *left* and with $EW(Ly\alpha) < 27$ Å on the *right panel* because this is one of the partitions leading to the strongest difference in Ext(Lyα - C). The error bars come from the background in the 2D stack at a spatial-direction position that is either higher or lower than the position of the science spectrum. The continuum is unresolved within the observation point spread function and the Lyα profile is more extended than the continuum profile.

This definition does not consider the difference in surface brightness of galaxies at different redshifts. This could be a limit of our approach. However, we emphasize that the median R magnitude and z_{sys} are very similar for all the subsets.

In Table 1, we show the properties of each subsample, such as the median systemic redshift, R magnitude, SFR, star formation rate surface density (Σ_{SFR}), stellar mass, and SiII velocity offset (Δv), equivalent width of the SiII1526 absorption line, CIII]1908, Lyα equivalent widths, Lyα spatial extension, and Lyα peak shift of the stacks. Star formation rate and stellar mass are obtained from the SED fitting; the star formation rate surface density (Heckman et al. 2015) is obtained from SFR and the PSF-corrected half-light-radius,

$$\Sigma_{SFR} \left[M_\odot \text{ yr}^{-1} \text{ kpc}^{-2} \right] = \frac{SFR}{2\pi r_{1/2}^2}, \qquad (5)$$

where $r_{1/2}$ is the PSF-corrected half-light radius of a galaxy as defined and estimated in Ribeiro et al. (2016).

The large error bar on the median stellar masses in the table indicate that the galaxies in each subset can be characterized by masses in the entire range of stellar masses, $\log(M_*/M_\odot) = [8.5–11]$.

3.4. Kinematics features

To quantify the ISM kinematics, we focused on the velocity offset between the central wavelength of the LIS lines and the systemic redshift of the stacked spectra. We chose the two absorption lines with the highest S/N in the majority of our stacked spectra, SiII1260 and SiII1526 (see Figs. A.1 and A.2).

We first set the systemic rest frame of the stacked spectrum in the following way. We fit the stacked-spectrum CIII]1908 line by assuming that the ratio between the fluxes of the lines of the doublet is 1.5 (Sect 2 Keenan et al. 1992)[4].

---

[4] An uncertainty in the flux ratio ($F(1907)/F(1909)$) of the CIII doublet could be translated into an uncertainty in the systemic redshift. As calculated in Keenan et al. (1992), $F(1907)/F(1909)$ varies from 1.5 to 0 for $1.5 < \log(n_e) < 6.5$ cm^{-3} and it is unchanged for $5000 < T_e < 20\,000$ K (their Fig. 1). For $\log(n_e) < 3.5$ cm^{-3}, the ratio is constant as $F(1907)/F(1909)=1.5$. Sanders et al. (2016) measured the electron density of a sample of $z \sim 2.3$ star-forming galaxies with SFRs that are consistent with those of our sample. By using the flux ratios of nebular

We assumed that the two SiII lines have the same velocity because they are transitions of the same element, but a different amplitude, and we searched for the best-fit velocity. We adopted the noise of the stacked spectrum in the minimization procedure.

The velocity offset between the LIS and the systemic redshift is calculated from the best-fit central wavelength of the SiII Gaussian fit, $l0_{best}(SiII)$,

$$\Delta v(SiII) = c \times \frac{l0_{best}(SiII) - l\_SiII_{air}\_z_{sys}}{l\_SiII_{air}\_z_{sys}}, \qquad (6)$$

where $l\_SiII_{air}\_z_{sys}$ is the theoretical wavelength of SiII in the air and c is the speed of light in km s^{-1}. There can be a significant negative value of $\Delta v(SiII)$. This is interpreted as the fact that the neutral gas is predominantly flowing out of the galaxy; there could be a gas component either at systemic redshift or inflowing, which is hidden within the outflowing gas. A $\Delta v(SiII)$ value consistent with 0 km s^{-1} can indicate either a static medium or a medium in which there are equal inflowing and outflowing gas components.

To estimate the errors on Δv, as well as on the equivalent widths, and Ext(Lyα-C), we also applied the bootstrap technique. As for the Lyα peak shift, we estimated the Gaussian-fit parameters in each fake realization and calculated the standard deviation among the 100 realizations. The standard deviation of $l0_{best}(SiII)$ provides the error on Δv.

4. Results

We present here the measurements obtained applying the methods described in Sect. 3. The measured quantities involved the 1D, such as equivalent widths, gas velocities, and Lyα peak shift, and 2D, such as Ext(Lyα-C), stacks. The scope of these measurements is to study simultaneously the Lyα spectral and spatial escape from the typical galaxy in each subset listed in Table 1.

Figure 6 shows the significance of the differences of the Lyα parameters and Δv within the pairs of subsamples. The subsamples of the galaxies that are faint and concentrated in the rest-frame UV characterized by $EW(CIII]1908) \geq 7.9$ Å have $EW(Ly\alpha)$ more than 2σ higher than the paired subsamples. The stacks of the galaxies located in overdense and underdense regions, and those of the most and the least massive galaxies show consistent $EW(Ly\alpha)$ values within the uncertainties.

Differences of the order of 2σ are observed for Δv, except for the pairs of subsets separated based on the median value of the stellar mass and the rest-frame UV concentration for which the velocity offsets are consistent. The galaxies brighter than $R = 24.5$ and more extended than the median in the rest-frame UV, which are characterized by $EW(Ly\alpha) < 27$ Å, $EW(CIII]1908) < 7.9$ Å, and localized in overdense regions, have a medium that is consistent with being static. The paired subsamples show a medium with a net flow out of the galaxy with a velocity larger than 300 km s^{-1}.

In terms of Ext(Lyα-C) and Lyα peak shift, differences within pairs can be observed, but tend to be less significant for some subsets. One of the limiting factors is that the spectra are obtained with VIMOS in low-resolution mode with a sampling of about 1 Å/pixel ($\sim$250 km s^{-1} at λLyα and $\sim$150 km s^{-1} at λCIII]1908). In addition, the sky subtraction technique (a

---

doublets, they infer a typical n_e of $\sim$250 cm^{-3} (their Fig. 3 and Sect. 3.4). Previous measurements had calculated values up to 1000 cm^{-3}, for which we can still adopt $F(1907)/F(1909) = 1.5$ (Talia et al. 2012) and infer a reliable z_{sys}.
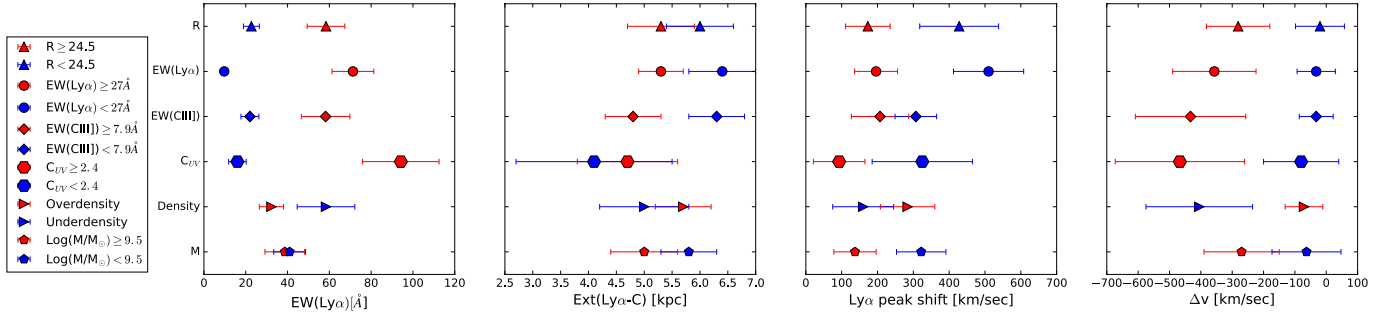
Fig. 6. Measurements of $EW(Ly\alpha)$ (*first panel*), Ext(Lyα-C) (*second panel*), Lyα peak shift (*third panel*), and Δv (*fourth panel*), together with the bootstrapping (see text) error bars for the subsamples listed in Table 1. The symbols correspond to the subsets listed in Table 1: galaxies fainter(brighter) than the median R magnitude of the entire sample are shown as red(blue) triangles; galaxies characterized by $EW(Ly\alpha)$ larger(smaller) than the median value are shown as red(blue) filled circles; galaxies characterized by $EW(CIII]1908)$ larger(smaller) than the median value as red(blue) diamonds; galaxies with rest-frame UV concentration larger(smaller) than the median value as red(blue) hexagons; galaxies with Ext(Lyα-C) larger(smaller) than the median value as red(blue) squares; galaxies in overdense(underdense) regions as red(blue) tilted triangles; and galaxies more(less) massive than the median value as red(blue) pentagons.
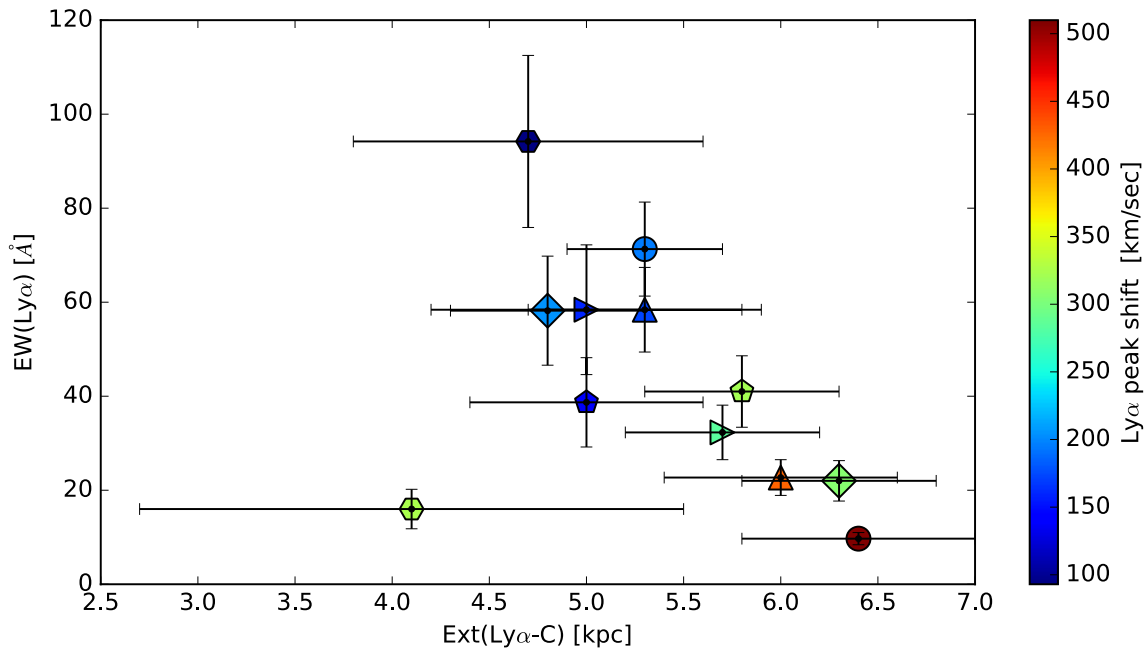

Fig. 7. Lyα equivalent width vs. Lyα spatial extension in kpc. The colour coding follows the values of the Lyα peak shift. The symbols represent the different subset listed in Table 1 as shown in Fig. 6.

low-order spline fit along the slit for each wavelength sampled; Le Fèvre et al. 2015) could produce an over subtraction near strong lines, such as a strong Lyα. The over subtraction (seen as negative pixel values) is particularly evident in stacked spectra and it can limit the accuracy of the spatial extent measurement. The difference of Ext(Lyα-C) we measure is generally of the order of 1σ. For the subsets of the most/least UV concentrated galaxies, the parameters are consistent. The stacks of the galaxies that are bright in the rest-frame UV, faint in Lyα, and less massive than the median are characterized by Lyα peak shifts 2σ larger than the UV faint, Lyα bright, and more massive galaxies.

In general, the error bars of all the measurements in the stacks of the most/least UV concentrated galaxies are large. One of the reasons is the smaller number of sources in comparison to the other subsamples.

Figure 7 is the most significant figure in the paper; this figure shows the three Lyα parameters that are outputs of the phenomena that allow the propagation inside and escape out of a galaxy. For the subsets for which the differences in the three parameters are significant (see Fig. 6), $EW(Ly\alpha)$ anti-correlates with Ext(Lyα-C) and Lyα peak shift. This trend is discussed in the following section. The bootstrap error bars of Ext(Lyα-C) for the galaxies with $C_{UV} < 2.4$ are the largest. Also, the galaxies in the $C_{UV} < 2.4$ subset are characterized by a larger variety of Lyα profiles and $EW(Ly\alpha)$ than the $C_{UV} \geq 2.4$ subset. The median of the $EW(Ly\alpha)$ measured in the individual spectra of the galaxies belonging to the $C_{UV} < 2.4$ subset is 13 ± 6 Å, while for the individual spectra of the galaxies in the $C_{UV} \geq 2.4$ subset is 83 ± 21 Å.

In Fig. 8, we wish to enlighten any possible trend between physical and Lyα properties. The first row of the figure shows that large outflow velocities seem to favour large values of $EW(Ly\alpha)$, small values of Ext(Lyα-C) and small Lyα peak shifts. In the following section, we discuss the role of outflows in the generation of a Lyα emission with certain values of equivalent width, spatial extension, and peak shift. Galaxies that are very concentrated and faint in the rest-frame UV have the largest outflow velocities ($\Delta v \geq 300$ km s^{-1}) and $EW(Ly\alpha) \geq 40$ Å.
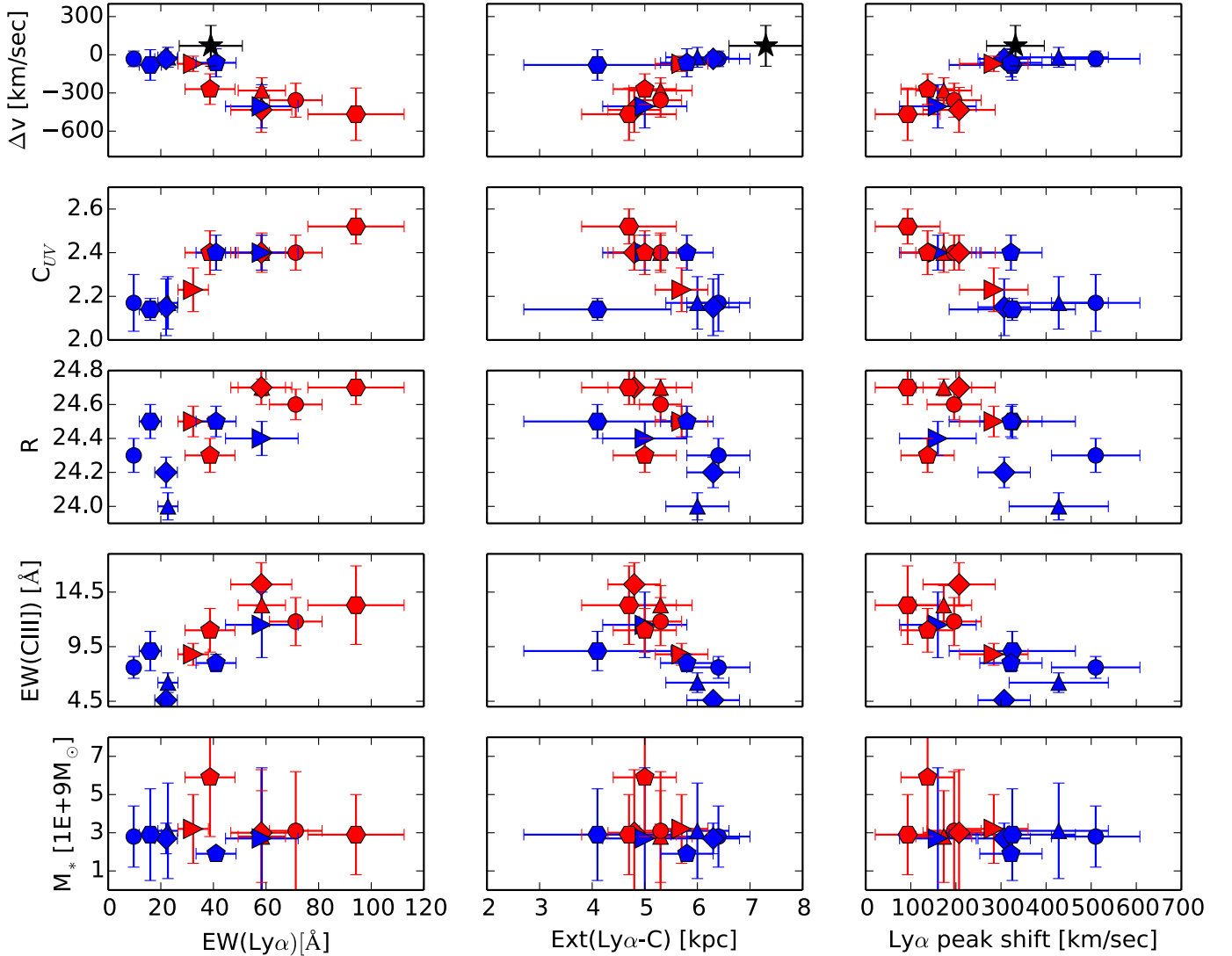
Fig. 8. Stack physical properties vs. Lyα properties. *From the top row*: the plots show Δ*v*, rest-frame UV concentration, rest-frame UV magnitude, *EW*(CIII]1908), and stellar mass vs. *EW*(Lyα) (*first column*), Ext(Lyα-C) (*second column*), and Lyα peak shift (*third column*). Symbols are as in Fig. 6. For each subset, Δ*v*, *EW*(Lyα), *EW*(CIII]1908), and Lyα peak shift are measured in the stacks, while C_{UV}, *R*, and M_* correspond to the median values of the galaxies within the subset. The black star represents a subset of sources with extreme Ext(Lyα-C) in the individual spectra. These sources are characterized by moderate *EW*(Lyα), Lyα peak shift larger than 300 km s^{-1} and Δ*v* consistent with zero.

5. Discussion

The aim of this work is to investigate the effect of HI gas kinematics and other gas/galaxy properties, such as the HI column density, on the escape and large-scale propagation of Lyα photons in star-forming galaxies. We investigate the gas kinematics in terms of the velocity of the outflowing HI gas and we study the dependency of the outflow velocity inferred by SiII as a function of the equivalent width, spatial extension, and red peak shift of Lyα with respect to the systemic redshift.

The Lyα photons emitted from galaxies that are bright in the rest-frame UV show larger Ext(Lyα-C) values and larger Lyα peak shifts than the paired subsets. Low-*EW*(CIII]1908) sources are characterized by a large HI column density and hence larger Ext(Lyα-C) values. These sources also show larger Lyα peak shifts than the subset of high-*EW*(CIII]1908) galaxies. We do not observe significant trends between Lyα properties and stellar mass.

Before interpreting the kinematics of the gas in the galaxies of our sample, we comment on the dependency of outflow velocity on star formation properties (Sect. 5.1). Then, we propose a model to explain our results (Sect. 5.2) and we interpret the observed trends in Sect. 5.3.

5.1. Star formation properties

Based on a simple model, when the pressure created by supernovae, stellar winds, and the radiation field from the star formation exceed the weight of the galaxy disk, an outflow can be launched perpendicular to the galactic plane. The strength of this outflow depends on the SFR per unit of area. Heckman (2001) proposed the existence of a Σ_{SFR} threshold above which a galaxy would be able to support outflows. Later on, they investigated the scaling relations of the outflow velocity with physical parameters and found that it weakly correlates with stellar mass, but strongly with SFR and Σ_{SFR} (Heckman et al. 2015; Alexandroff et al. 2015; Heckman & Borthakur 2016). Newman et al. (2012) studied the kinematics in a sample of $z \sim 2$ star-forming galaxies

with SFRs from a few tens to a few hundreds of $M_\odot$ yr^{-1} and M_* of the order of 2–100×10^9 $M_\odot$. They found that the strongest outflows are observed for massive ($M_* > 10^{10}$ $M_\odot$), high-SFR ($SFR > 100$ $M_\odot$ yr^{-1}), compact ($r_{1/2} < 3$ kpc), face-on galaxies, which, by consequence, are characterized by $\Sigma_{SFR} > 1$ $M_\odot$ yr^{-1} kpc^{-2}. Chisholm et al. (2015) showed that the strongest outflows can also arise from merging events.

In Table 1, we report the median values of SFR and SFR per unit of area, obtained from the same definition in Heckman et al. (2015). We do not see a clear proportionality between Σ_{SFR} and outflow velocity. However, we can see that in the subsamples for which the difference between the Δv values are more significant, there are also notable differences in the Σ_{SFR} values. In particular a higher value of Δv is related to a higher value of Σ_{SFR} (first three rows of Table 1).

The SFR and size conditions of the typical galaxy of our subsamples could allow the formation of outflows and we want to investigate how much they contribute to the escape and propagation of Lyα photons.

5.2. Theoretical model

We compare our observational results with the theoretical model by Verhamme et al. (2006). We chose this model because it allows us to predict the quantities we are considering in this work, such as Lyα equivalent width, spatial extension, and peak shift, with respect to HI column density and outflow velocity.

The model predicts the shape of the Lyα emission line, by assuming an expanding, spherical, homogeneous, and isothermal shell of neutral hydrogen surrounding a central starburst. The stars emit UV continuum and the Lyα radiation is produced in the ISM. The expanding shell is characterized by an expansion velocity, $V_{\rm exp}$, which can mimic the outflow velocity. By following a Monte Carlo approach, Lyα photons follow a random path encountering HI atoms and dust grains. The model produces the Lyα spectrum out of the galaxy depending on the shell parameters, such as $V_{\rm exp}$, HI column density, and dust absorption optical depth.

For increasing HI column density, the Lyα main peak is increasingly red-shifted (Verhamme et al. 2015). However, outflow velocities larger than 300 km s^{-1} could allow some of the Lyα photons to escape at the systemic redshift (the Lyα peak would be significantly red-shifted if $N_{\rm HI} > 10^{20}$ cm^{-2}; see Fig. 2 in Verhamme et al. 2015). An HI gas characterized by those high velocities and low to moderate $N_{\rm HI}$ is not efficient in scattering Lyα photons. As a consequence, the majority of the Lyα flux is peaked in the center of the galaxy and does not produce an extended Lyα spatial profile. The models from Barnes & Haehnelt (2010) also indicate that the Lyα emission becomes more centrally peaked with the increase of the velocity of the HI bulk (see also Gronke & Dijkstra 2016).

With the Verhamme et al. (2006) model, it is possible to study Lyα spatial extension and equivalent width at given shell parameters. The model predicts that the Lyα spatial extension is proportional to $N_{\rm HI}$ and depends on the scattering capability of the HI gas. For $N_{\rm HI} > 10^{19}$ cm^{-2}, the scattering is efficient. So, a very large $V_{\rm exp}$ would be needed to make a compact Lyα emission. For $N_{\rm HI} < 10^{19}$ cm^{-2}, the Lyα emission is spatially compact independently on $V_{\rm exp}$ (Verhamme et al., in prep.). Also, it is possible to predict that $EW({\rm Ly}\alpha)$ increases when the optical depth of the ISM decreases. Since dust completely absorbs Lyα photons, it reduces the amount of photons coming out towards the center and those that are distributed on a large scale. As a

consequence $EW({\rm Ly}\alpha)$ and Ext(Lyα-C) decreases. On the other hand, the HI gas scatters Lyα photons away from the line of sight (Verhamme et al. in prep.).

5.3. Interpretation of the observed small outflow velocity, small Lyα equivalent width, and large Lyα spatial extension

As described in Sect. 4, the subsamples of the galaxies that are bright in UV and faint in Lyα show Lyα peak shifts up to 500 km s^{-1}, Ext(Lyα-C) larger than 6 kpc, $EW({\rm Ly}\alpha) < 40$ Å, and are characterized by Δv that is consistent with a static medium. Instead, the subsamples of R faint and Lyα bright galaxies, characterized by large Δv, and therefore large outflow velocities, present the Lyα red peak close to the systemic redshift, less extended Lyα spatial profiles, and larger Lyα equivalent widths. These behaviours are also seen for the subsamples that are separated based on rest-frame UV concentration and local density. In particular, for the most compact galaxies we measured Δv consistent with an outflowing gas and larger $EW({\rm Ly}\alpha)$ than for the least compact. The galaxies located in underdense regions present larger Δv, Lyα peak shift, Ext(Lyα-C), and smaller $EW({\rm Ly}\alpha)$ than the galaxies located in overdense regions. For a subset of 10 galaxies with extreme Ext(Lyα-C) values (black stars in Fig. 8), we measure a Δv value consistent with a static medium and $EW({\rm Ly}\alpha) = 40$ Å.

From the first row of Fig. 8, we can see that kinematics is important for the propagation and escape of Lyα photons. However, to investigate if the kinematics alone is enough to explain the trend of large Lyα peak shift, large Ext(Lyα-C), and small $EW({\rm Ly}\alpha)$, we compare our results with the theoretical models by Verhamme et al. (2006, Sect. 5.2). We first simulate the 1D Lyα emission line for different shell expansion velocities and for three HI column densities (Fig. 9 upper row). Expansion velocities of 50–400 km s^{-1} would produce near-overlapping Lyα peaks if the spectral resolution were comparable to that of VUDS ($R \leq 300$) and $N_{\rm HI} \leq 10^{19}$ cm^{-2}. This tells us that the kinematics alone would have an effect that is too small on the Lyα peak shifts to be seen at VUDS resolution. For small HI column densities, shift differences of the order of 100 km s^{-1} are not discernible. Increasing $N_{\rm HI}$, the separation between Lyα peaks at different $V_{\rm exp}$ enlarges. In this model, the effect of the intergalactic medium (IGM) on the shape of the Lyα line is not included. It has been shown that the effect of the IGM is marginal in comparison to that of the ISM, even more if the ISM gas is already outflowing (e.g. Dijkstra 2016). In fact, a typical red shift of the Lyα line is also seen in star-forming galaxies in the local Universe (Orlitova et al. in prep; Henry et al. 2015; Verhamme et al. 2017; Yang et al. 2017, for already published examples). The correlation between Ext(Lyα-C) and Lyα peak shift also tells us that Lyα photons are produced within the galaxy.

Then, we simulate the same line by varying the HI column density (Fig. 9, lower row). The Lyα peak shift is much larger than the expansion velocity. For velocities of 50–200–300 km s^{-1} and $N_{\rm HI} \sim 10^{21}$ cm^{-2}, the Lyα peak shift is even larger than 1000 km s^{-1}. Variations of 500 km s^{-1} in the shift of the Lyα peak could be related to a $\Delta \log(N_{\rm HI}) = 2$. At VUDS resolution, the strongest variations in the location of the Lyα peak shift are therefore probably due to variations in $N_{\rm HI}$. The profiles in Fig. 9 are shown for stellar reddening, $E(B-V) = 0.0$. The inclusion of dust in the simulation would reduce the entire Lyα flux, preserving the way the Lyα profile changes when $N_{\rm HI}$ and $V_{\rm exp}$ vary.
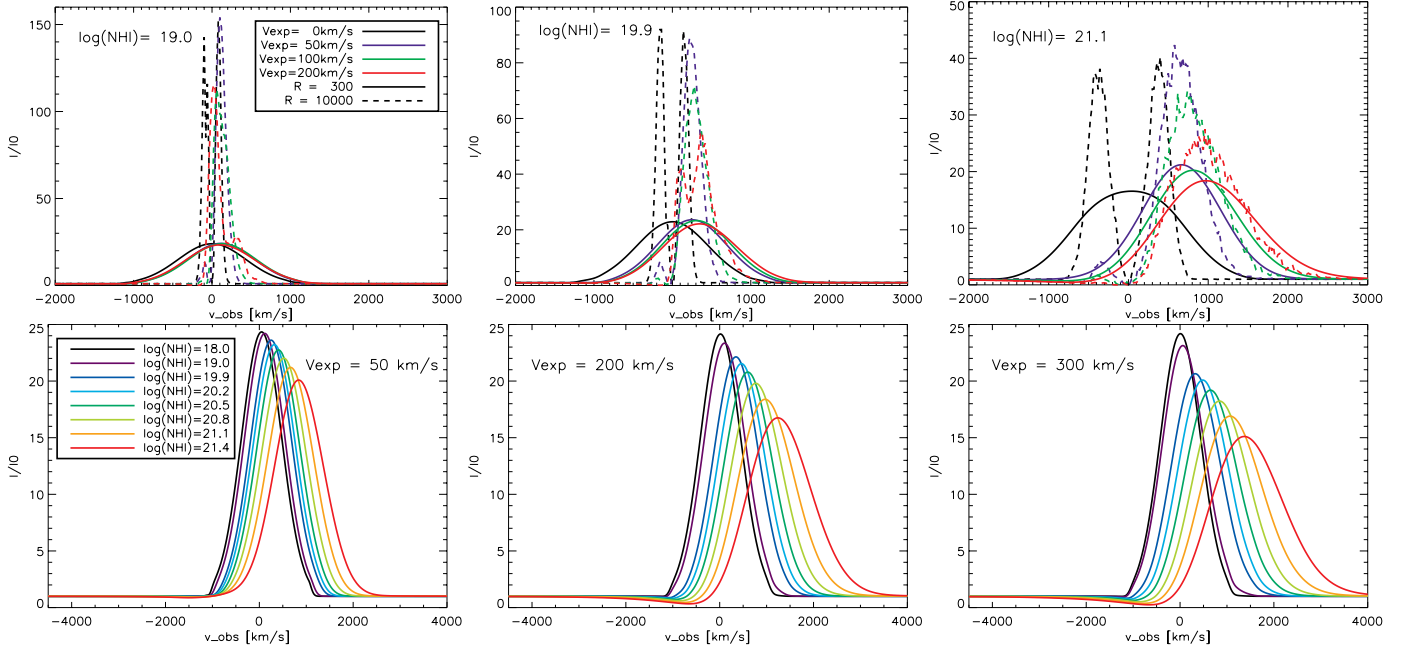
Fig. 9. Theoretical 1D Lyα emission line (in velocity space) profiles obtained with the adopted (dust-free) shell model. The Lyα profiles (I) are normalized to the level of the continuum (I0). The maximum resolution profiles are shown as dashed lines. Solid lines correspond to VUDS resolution, $R \sim 300$. *Upper row*: we assumed different shell expansion velocities and three HI column densities, $\log(N_{HI}) = 19$ (*left panel*), 20 (*middle panel*), and 21 (*right panel*). *Lower row*: we assumed different values of HI column density and three shell expansion velocities, $V_{exp} = 50$ (*left panel*), 200 (*middle panel*), and 300 (*right panel*) km s^{-1}.

Our data show that for the subsamples with Δv smaller than 100 km s^{-1} and Lyα peak shifts larger than 300 km s^{-1}, Ext(Lyα-C) is larger than 5 kpc. These values can be explained with $N_{HI} = 10^{20}$–10^{21} cm^{-2} in the framework of the shell model. The scattering of the gas with this N_{HI} would favour low $EW(Ly\alpha)$. On the other hand, for the subsample with Δv larger than 300 km s^{-1} and Lyα peak shifts smaller than 300 km s^{-1}, Ext(Lyα-C) is less than 5 kpc. This is consistent with a $N_{HI} < 10^{20}$ cm^{-2} gas. In this case we could expect a large $EW(Ly\alpha)$.

If kinematics alone was the main cause of the three Lyα properties, we would note a large Lyα peak shift and Lyα spatial extension in the cases of large outflow velocities. This is not observed in our data. Therefore, the HI column density has a key role in shaping the Lyα emission.

In Fig. 7 and 8, we show that extended Lyα spatial profiles are most likely to be produced by scattered light. They could also be due to the ionization of the external shell of the circum-galactic medium by the UV background, which recombines and emits Lyα in situ as fluorescence (e.g. Kollmeier et al. 2010; Cantalupo et al. 2012). Another scenario is that of the gravitational cooling of the gas falling onto galaxies (e.g. Rosdahl & Blaizot 2012), which may also lead to some level of scattering of the Lyα photons on their way out. This happens since the Lyα emissivity is proportional to the density, i.e. higher at the center. The scattering process naturally links the spatial extent with the shift of the Lyα peak and the small $EW(Ly\alpha)$. The fluorescence and gravitational cooling scenarios can explain any Lyα spatial extension, but does not explain the correlation with the shift of the peak nor with the equivalent width.

Here, we considered the interpretation of the data from homogeneous shell models, but it remains to be studied if other geometries would also show the same behaviour. According to Verhamme et al. (2015), a scattering medium with holes would produce the direct escape of Lyα photons and hence lines at systemic redshift. Our data do not seem to favour the presence of

holes. According to Gronke & Dijkstra (2016), clumpy outflows decrease the effective optical depth seen by the Lyα photons compared to the "real" column density seen by non-resonant photons along the line of sight, and lead to a small peak shift and boosted escape fraction in comparison to a homogeneous medium of the same outflow velocity and same column density. It remains to be studied if a correlation with the spatial extension, as observed in Fig. 7, would be conserved by clumpy geometries.

The galaxies in our sample characterized by a large N_{HI} ($N_{HI} \simeq 10^{20}$ cm^{-2}) would be those with Δv that is consistent with a static medium, which is bright in UV, faint in Lyα with $C_{UV} < 2.4$, localized in overdense regions, and that has most extended Lyα spatial profiles. This means that Lyα properties are clearly related to some galactic properties and so that Lyα photons are mainly produced inside the ISM. We find that concentration has the strongest impact on kinematics and that there is a clear (anti-)correlation between Lyα and rest-frame UV concentration.

Results in the literature (e.g. Verhamme et al. 2008; Hashimoto et al. 2015) have shown that the star-forming galaxies that are bright in UV, faint in Lyα, and more extended in the rest-frame UV are also more massive. It is not surprising that they could also be characterized by large HI amount and possibly N_{HI}. In addition to this, we find that LAEs are characterized by outflow velocities of 200–500 km s^{-2} and Lyα peak shift of 100–300 km s^{-2}. This is in agreement with the findings in Verhamme et al. (2015), in which they explained that the shift of the Lyα red peak can be related but is not directly proportional to the velocity of the outflowing shell. Rest-frame UV compact sources also tend to be characterized (on average) by outflows of large velocities, which could be favoured by the small size under the same star formation rate activity.

An important consequence of the interpretation of our results is that it is possible to use Lyα emission to trace the HI gas and hence infer about the processes that can regulate the distribution

and kinematics of the gas into and out of galaxies during their evolution. If Lyα emitters are characterized by strong outflows and low HI column densities, it is possible that they are seen in moments in which they are experiencing very active phases of star formation that consume the gas very fast (see also A17).

It is, also, interesting and could have implication for the epoch of the re-ionization (Stark et al. 2015), that galaxies with larger EW(Lyα) and EW(CIII]1908) are also those with smaller Ext(Lyα-C) and smaller Lyα peak shifts on average. In fact, at $z \simeq 7$ Lyα peak shifts of the order of 200 km s^{-1} could be interpreted as the fact that the intergalactic medium is still ionized (see also Pentericci et al. 2016).

5.4. Comparison with previous studies

The role of kinematics and HI column density in conditioning the escape of Lyα photons and in shaping the Lyα emission line was studied in detail in high-resolution spectra. Hashimoto et al. (2015) found that the $z \simeq 2.2$ Lyα emitters of their sample with Lyα peaks close to the systemic redshift had properties consistent with an $N_{HI} < 10^{19}$ cm^{-2}. Moreover, they observed an anti-correlation between N_{HI} and Lyα peak shift. Erb et al. (2014), Trainor et al. (2015) proposed that the shape of the Lyα line at $z \sim 2$–3 is mainly due to the gas column density and covering fraction, while the kinematics would mostly affect the line wings (see also Steidel et al. 2010). Also, they found no evidence that the shift of the Lyα peak is directly proportional to the outflow velocity and that the Lyα peak shift anti-correlates with EW(Lyα) (see also Shibuya et al. 2014b). These observations are consistent with our results.

At low redshift, the escape of Lyα photons was extensively studied using the Cosmic Origins Spectrograph (COS) on board the *Hubble* Space Telescope (HST). Observations of local UV-selected galaxies from the Lyα Reference Sample (LARS; Östlin et al. 2014) and Green Pea galaxies (Cardamone et al. 2009), a sample of compact, metal-poor starbursts at $z \simeq 0.1$–0.3 that are good analogues of high-redshift LAEs (Amorín et al. 2010, 2012; Jaskot & Oey 2013), have shown that outflows are a necessary but not sufficient condition for the Lyα photons to escape star-forming regions (Rivera-Thorsen et al. 2015; Henry et al. 2015). Yang et al. (2016) discovered a significant anti-correlation between Lyα escape fraction and N_{HI} by means of fitting the Lyα emission line profile of Green Pea spectra with shell models. Yang et al. (2017) extracted the Lyα spatial extension from the 2D COS spectra and showed a trend for which large escape fraction values correspond to compact Lyα morphology. Our results at high redshift are in agreement with these trends.

The measurements for the subsamples based on density can tell us that large equivalent width Lyα emitting galaxies tend to prefer underdense regions, where they also seem to support larger outflow velocities. Galaxies with lower EW(Lyα) would be mainly located in overdense regions and would be characterized by larger scale Lyα emissions. We speculate that galaxy-galaxy interactions in overdense regions could increase the column density of the HI gas in the close circum-galactic medium. That gas would be able to scatter Lyα photons and reproduce our results. Matsuda et al. (2012), Momose et al. (2016) showed that the size of the Lyα spatial extension is indeed proportional to the density. Gronke & Dijkstra (2016) explored the effect of cold HI and hot HII gas on the Lyα emission. According to their model, the suppression of the flux in the line center and the extended Lyα spatial profile could also be produced by the properties of the gas in the circum-galactic medium.

Cooke et al. (2013) identified Lyα as an environment diagnostic. They found that the star-forming galaxies tend to show Lyα in absorption in massive, group-like halos, while Lyα in emission tends to be observed for galaxies in the outskirts of massive halos, maybe on top of filamentary structures. Our results are also in agreement with these observations.

To summarize, our results are consistent with a scenario in which the ISM kinematics helps the escape of Lyα photons in the sense that the EW(Lyα) could be larger than 40 Å, the Lyα peak is red-shifted with respect to the systemic redshift, and the Lyα spatial extension is larger than the continuum. However, an $N_{HI} > 10^{20}$ cm^{-2} can produce Lyα peak shifts larger than 300 km s^{-1} and could allow Ext(Lyα-C) to be up to 7 kpc, especially in a static ISM. There is evidence that kinematics and N_{HI} both contribute to explain the trends we see. However, the outflow velocity seems to mainly contribute to EW(Lyα) and the outflow velocity, together with N_{HI}, also explain the Lyα line shape and large-scale spatial extension. Combined with recent results in the literature, the low NHI together with low metallicity and high-ionization capability would make a galaxy a strong Lyα emitter (Trainor et al. 2016).

6. Conclusions

In this work, we have considered a sample of Lyα emitting galaxies from VUDS. We chose the range of redshift of $2 < z < 4$ to be able to study the Lyα emission line and the systemic-redshift sensitive features within one single rest-frame UV spectrum (Sect. 2). This avoids the wavelength calibration uncertainty that is sometimes related to using optical data to study rest-frame UV lines and NIR spectra to infer z_{sys}. We measured the systemic redshift of the individual galaxies from the CIII]1908 emission line and we obtained stacked spectra of subsamples of galaxies based on the spectroscopic and physical properties listed in the first column of Table 1. Therefore, the sample of sources we consider is composed of Lyα+ CIII] emitters. These sources share the same typical stellar mass and stellar mass density as the typical Lyα emitting galaxies in VUDS and are characterized by larger EW(Lyα).

From the stacked spectra, we derived the HI outflow velocities by measuring the velocity offset, Δv, between the systemic redshift and the mean of the Gaussian best fit of the low-ionization absorption lines (SiII1260 and SiII1526). Also, we studied the spatial extension of the Lyα profile, Ext(Lyα-C), from the 2D spectra (Sect. 3).

In Table 1 and Figs. 6–8, we summarize the main results of our analysis, which are as follows:

- The typical galaxies in our subsamples have the Σ_{SFR} conditions to support outflows.
- The subsamples for which we measured large Lyα peak shifts (>300 km s^{-1}), extended Lyα spatial profiles (up to 7 kpc more extended than the UV continuum, based on our definition), and small EW(Lyα) are characterized by Δv(SiII) that is either consistent with a static medium or a medium with an equal contribution of inflows and outflows.
- The subsample of rest-frame UV faint Lyα emitters present less extended Lyα spatial profiles, small Lyα peak shifts, and we measure velocity offsets consistent with outflow velocities of a few hundreds of km s^{-1}. Also they tend to prefer underdense regions.
- By combining our results with the predictions from the radiative-transfer model we can observe that, at VUDS

resolution, we are able to notice the effect of HI column density in the escape and spatial extension of Lyα photons.

- From the comparison with the model predictions, we can say that a Lyα peak shift larger than 300 km s^{-1} can be observed from an ISM with HI column density more than 10^{20} cm^{-2}. This value of $N_{\rm HI}$ would favour an efficient scattering process even in the case of a static medium. With the large $N_{\rm HI}$ we can also explain the large Lyα extension and the small $EW(Ly\alpha)$. On the other hand, a large Δv would imply a Lyα spatial profile that is peaked in the galaxy center (i.e. low values of Ext(Lyα-C)), and therefore a large $EW(Ly\alpha)$, as in our data.

- The sources that are more compact in the rest-frame UV are characterized by larger outflow velocities than the paired sample. The galaxies preferentially located in overdense regions also present larger Ext(Lyα-C) values than the paired sample. We speculate that this can be produced by galaxy-galaxy interactions, which could increase the $N_{\rm HI}$ in the close circum-galactic medium.

- Our results and their interpretation via radiative-transfer models tell us that it is possible to use Lyα to trace the properties of the HI gas. Also, the fact that Lyα emitters are characterized by large Δv could give hints about their stage of evolution. They could be experiencing short bursts of star formation that push strong outflows. More massive star-forming galaxies could be experiencing more normal phases of star formation, which slowly consume the HI gas, and could be showing extended Lyα spatial profiles favoured by the larger HI column density.

- We have shown in Fig. 7 the correlation between Lyα spatial and spectral escape from galaxies. It is expected in case of scattering processes. This implies that the origin of the extended Lyα spatial profiles is the scattered light.

To confirm the role of kinematics and of HI column density in favouring the escape and distribution of Lyα photons, we will study higher resolution spectra of galaxies from the VANDELS[5] survey. The VANDELS survey aims to deliver very deep VIMOS spectra (at least 20 h exposure on source with a maximum of 80 h) of bright $2.5 < z < 5.5$ and faint $2.5 < z < 7$ star-forming galaxies. We will be able to detect systemic-redshift sensitive features and LIS lines with enough S/N to study kinematics in individual spectra. The HI amount and distribution can be different in different density environments. Therefore, within VANDELS we will also study Lyα as a function of environment and infer the processes that can regulate the distribution and kinematics of the gas into and out of galaxies during their evolution.

References

Alexandroff, R. M., Heckman, T. M., Borthakur, S., Overzier, R., & Leitherer, C. 2015, ApJ, 810, 104

Amorín, R. O., Pérez-Montero, E., & Vílchez, J. M. 2010, ApJ, 715, L128

Amorín, R., Pérez-Montero, E., Vílchez, J. M., & Papaderos, P. 2012, ApJ, 749, 185

Amorín, R., Fontana, A., Pérez-Montero, E., et al. 2017, Nat. Astron., 1, 0052

Arnouts, S., Cristiani, S., Moscardini, L., et al. 1999, MNRAS, 310, 540

Barnes, L. A., & Haehnelt, M. G. 2010, MNRAS, 403, 870

Bruzual, G., & Charlot, S. 2003, MNRAS, 344, 1000

Cantalupo, S., Lilly, S. J., & Haehnelt, M. G. 2012, MNRAS, 425, 1992

Cardamone, C., Schawinski, K., Sarzi, M., et al. 2009, MNRAS, 399, 1191

Cassata, P., Tasca, L. A. M., Le Fèvre, O., et al. 2015, A&A, 573, A24

Chabrier, G. 2003, PASP, 115, 763

Chiappetti, L., Tajer, M., Trinchieri, G., et al. 2005, A&A, 439, 413

Chisholm, J., Tremonti, C. A., Leitherer, C., et al. 2015, ApJ, 811, 149

Civano, F., Elvis, M., Brusa, M., et al. 2012, ApJS, 201, 30

Civano, F., Marchesi, S., Comastri, A., et al. 2016, ApJ, 819, 62

Cooke, J., Omori, Y., & Ryan-Weber, E. V. 2013, MNRAS, 433, 2122

Dijkstra, M. 2016, in Understanding the Epoch of Cosmic Reionization: Challenges and Progress, ed. A. Mesinger, Astrophys. Space Sci. Libr., 423, 145

Dijkstra, M., Haiman, Z., & Spaans, M. 2006, ApJ, 649, 14

Duval, F., Schaerer, D., Östlin, G., & Laursen, P. 2014, A&A, 562, A52

Erb, D. K., Pettini, M., Shapley, A. E., et al. 2010, ApJ, 719, 1168

Erb, D. K., Steidel, C. C., Trainor, R. F., et al. 2014, ApJ, 795, 33

Feltre, A., Charlot, S., & Gutkin, J. 2016, MNRAS, 456, 3354

Finkelstein, S. L., Hill, G. J., Gebhardt, K., et al. 2011, ApJ, 729, 140

Fiore, F., Puccetti, S., Grazian, A., et al. 2012, A&A, 537, A16

Gawiser, E., Francke, H., Lai, K., et al. 2007, ApJ, 671, 278

Grogin, N. A., Kocevski, D. D., Faber, S. M., et al. 2011, ApJS, 197, 35

Gronke, M., & Dijkstra, M. 2016, ApJ, 826, 14

Gronwall, C., Ciardullo, R., Hickey, T., et al. 2007, ApJ, 667, 79

Guaita, L., Acquaviva, V., Padilla, N., et al. 2011, ApJ, 733, 114

Guaita, L., Francke, H., Gawiser, E., et al. 2013, A&A, 551, A93

Guaita, L., Melinder, J., Hayes, M., et al. 2015, A&A, 576, A51

Hagen, A., Ciardullo, R., Gronwall, C., et al. 2014, ApJ, 786, 59

Hashimoto, T., Ouchi, M., Shimasaku, K., et al. 2013, ApJ, 765, 70

Hashimoto, T., Verhamme, A., Ouchi, M., et al. 2015, ApJ, 812, 157

Hathi, N. P., Le Fèvre, O., Ilbert, O., et al. 2016, A&A, 588, A26

Hayes, M., Östlin, G., Schaerer, D., et al. 2013, ApJ, 765, L27

Hayes, M., Östlin, G., Duval, F., et al. 2014, ApJ, 782, 6

Heckman, T. M. 2001, in Gas and Galaxy Evolution, eds. J. E. Hibbard, M. Rupen, & J. H. van Gorkom, ASP Conf. Ser., 240, 345

Heckman, T. M., & Borthakur, S. 2016, ApJ, 822, 9

Heckman, T. M., Alexandroff, R. M., Borthakur, S., Overzier, R., & Leitherer, C. 2015, ApJ, 809, 147

Henry, A., Scarlata, C., Martin, C. L., & Erb, D. 2015, ApJ, 809, 19

Huang, K.-H., Lemaux, B. C., Schmidt, K. B., et al. 2016, ApJ, 823, L14

Ilbert, O., Capak, P., Salvato, M., et al. 2009, ApJ, 690, 1236

Jaskot, A. E., & Oey, M. S. 2013, ApJ, 766, 91

Jaskot, A. E., & Ravindranath, S. 2016, ApJ, 833, 136

Kalfountzou, E., Civano, F., Elvis, M., Trichas, M., & Green, P. 2014, MNRAS, 445, 1430

Keenan, F. P., Feibelman, W. A., & Berrington, K. A. 1992, ApJ, 389, 443

Kim, M., Kim, D.-W., Wilkes, B. J., et al. 2007, ApJS, 169, 401

Koekemoer, A. M., Aussel, H., Calzetti, D., et al. 2007, ApJS, 172, 196

Koekemoer, A. M., Faber, S. M., Ferguson, H. C., et al. 2011, ApJS, 197, 36

Kollmeier, J. A., Zheng, Z., Davé, R., et al. 2010, ApJ, 708, 1048

Kornei, K. A., Shapley, A. E., Erb, D. K., et al. 2010, ApJ, 711, 693

Laursen, P., Sommer-Larsen, J., & Razoumov, A. O. 2011, ApJ, 728, 52

Le Fèvre, O., Tasca, L. A. M., Cassata, P., et al. 2015, A&A, 576, A79

Lemaux, B. C., Tomczak, A. R., Lubin, L. M., et al. 2016, MNRAS, 472, 419

Matsuda, Y., Yamada, T., Hayashino, T., et al. 2012, MNRAS, 425, 878

Momose, R., Ouchi, M., Nakajima, K., et al. 2014, MNRAS, 442, 110

Momose, R., Ouchi, M., Nakajima, K., et al. 2016, MNRAS, 457, 2318

Nakajima, K., Ellis, R. S., Iwata, I., et al. 2016, ApJ, 831, L9

Nakajima, K., Ouchi, M., Shimasaku, K., et al. 2012, ApJ, 745, 12

Nakajima, K., Ouchi, M., Shimasaku, K., et al. 2013, ApJ, 769, 3

Neufeld, D. A. 1990, ApJ, 350, 216

Newman, S. F., Genzel, R., Förster-Schreiber, N. M., et al. 2012, ApJ, 761, 43

Orsi, A., Lacey, C. G., & Baugh, C. M. 2012, MNRAS, 425, 87

Östlin, G., Hayes, M., Duval, F., et al. 2014, ApJ, 797, 11

Pardy, S. A., Cannon, J. M., Östlin, G., et al. 2014, ApJ, 794, 101

Pentericci, L., Carniani, S., Castellano, M., et al. 2016, ApJ, 829, L11

Ribeiro, B., Le Fèvre, O., Tasca, L. A. M., et al. 2016, A&A, 593, A22

Rigby, J. R., Bayliss, M. B., Gladders, M. D., et al. 2015, ApJ, 814, L6

Rivera-Thorsen, T. E., Hayes, M., Östlin, G., et al. 2015, ApJ, 805, 14

Rosdahl, J., & Blaizot, J. 2012, MNRAS, 423, 344

Sanders, R. L., Shapley, A. E., Kriek, M., et al. 2016, ApJ, 816, 23

Schaerer, D., Hayes, M., Verhamme, A., & Teyssier, R. 2011, A&A, 531, A12

Shibuya, T., Ouchi, M., Nakajima, K., et al. 2014a, ApJ, 788, 74

---

[5] http://vandels.inaf.it/

Shibuya, T., Ouchi, M., Nakajima, K., et al. 2014b, ApJ, 785, 64
Smit, R., Bouwens, R. J., Labbé, I., et al. 2014, ApJ, 784, 58
Smit, R., Swinbank, A. M., Massey, R., et al. 2017, MNRAS, 467, 3306
Stark, D. P., Richard, J., Siana, B., et al. 2014, MNRAS, 445, 3200
Stark, D. P., Richard, J., Charlot, S., et al. 2015, MNRAS, 450, 1846
Stark, D. P., Ellis, R. S., Charlot, S., et al. 2017, MNRAS, 464, 469
Steidel, C. C., Erb, D. K., Shapley, A. E., et al. 2010, ApJ, 717, 289
Steidel, C. C., Bogosavljević, M., Shapley, A. E., et al. 2011, ApJ, 736, 160
Talia, M., Mignoli, M., Cimatti, A., et al. 2012, A&A, 539, A61
Tasca, L. A. M., Le Fèvre, O., Ribeiro, B., et al. 2017, A&A, 600, A110
Trainor, R. F., Steidel, C. C., Strom, A. L., & Rudie, G. C. 2015, ApJ, 809, 89

Trainor, R. F., Strom, A. L., Steidel, C. C., & Rudie, G. C. 2016, ApJ, 832, 171
Vargas, C. J., Bish, H., Acquaviva, V., et al. 2014, ApJ, 783, 26
Verhamme, A., Schaerer, D., & Maselli, A. 2006, A&A, 460, 397
Verhamme, A., Schaerer, D., Atek, H., & Tapken, C. 2008, A&A, 491, 89
Verhamme, A., Orlitová, I., Schaerer, D., & Hayes, M. 2015, A&A, 578, A7
Verhamme, A., Orlitová, I., Schaerer, D., et al. 2017, A&A, 597, A13
Wisotzki, L., Bacon, R., Blaizot, J., et al. 2016, A&A, 587, A98
Xue, Y. Q., Luo, B., Brandt, W. N., et al. 2011, ApJS, 195, 10
Yang, H., Malhotra, S., Gronke, M., et al. 2016, ApJ, 820, 130
Yang, H., Malhotra, S., Rhoads, J. E., et al. 2017, ApJ, 838, 4
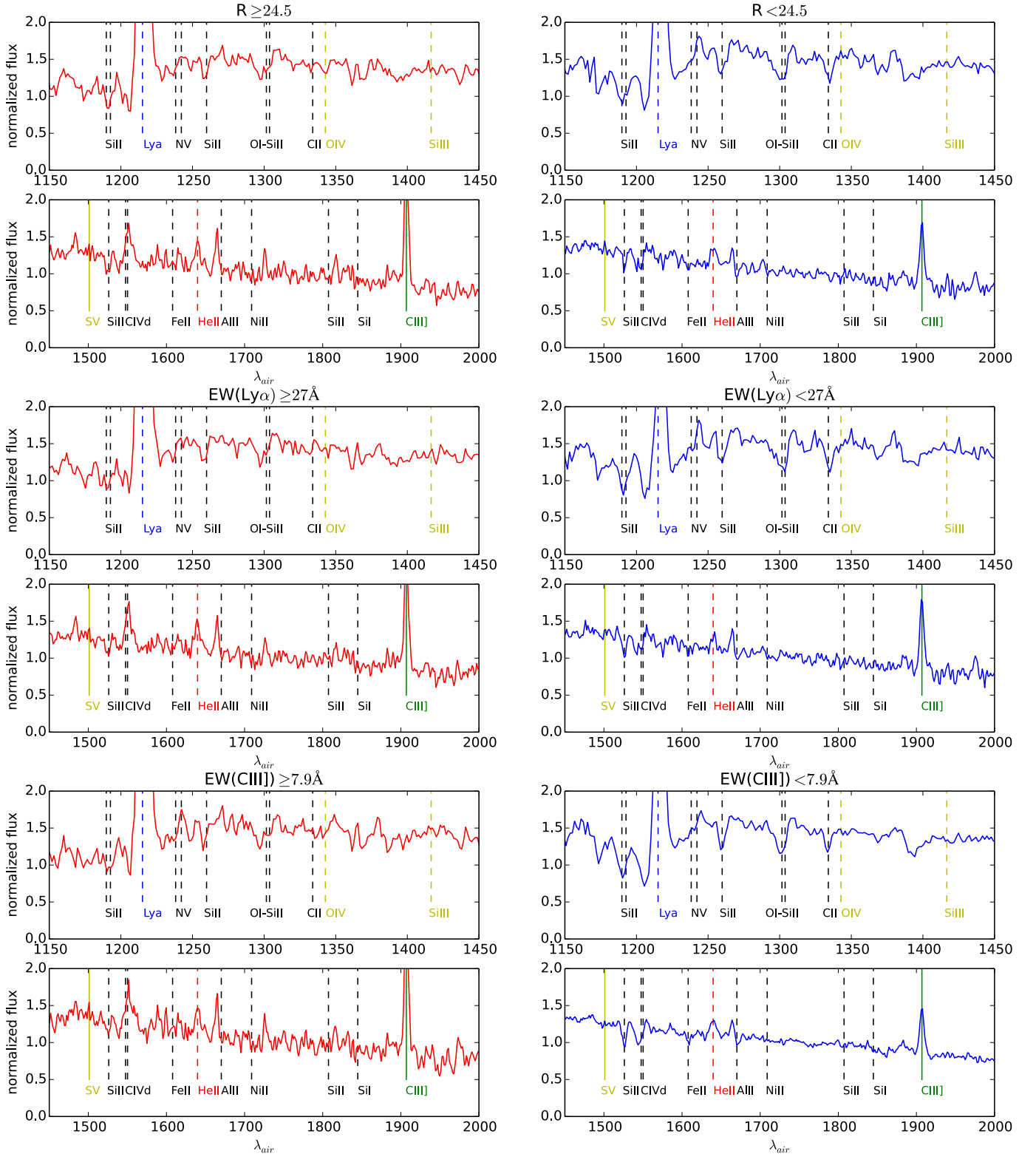Zheng, Z.-Y., Malhotra, S., Rhoads, J. E., et al. 2016, ApJS, 226, 23

Fig. A.1. Stacked spectra of the subsamples of the galaxies with $R \geq 24.5$ and $R < 24.5$, $EW(Ly\alpha) \geq 27$ Å and $EW(Ly\alpha) < 27$ Å, $EW(CIII]1908) \geq 7.9$ Å and $EW(CIII]19078) < 7.9$ Å. For each subsample we present *two panels*, one covering the wavelength region with Lyα (*upper*) and the other the wavelength region with CIII]1908 (*lower*).

Appendix A: Stacked spectra of the subsamples reported in Table 1

The following figures show the stacked spectra of the galaxies of each subsample. Stellar features are indicated with yellow, ISM absorption lines with black dashed lines. We clearly see the Lyα (blue dashed line) and CIII]1908 (green dashed line) emission lines. We can see the HeII (red dashed line) at the z_{sys} of the stacks. We verified that the emission line ratios are consistent with those of SFGs (not AGNs) based on the models in Feltre et al. (2016).
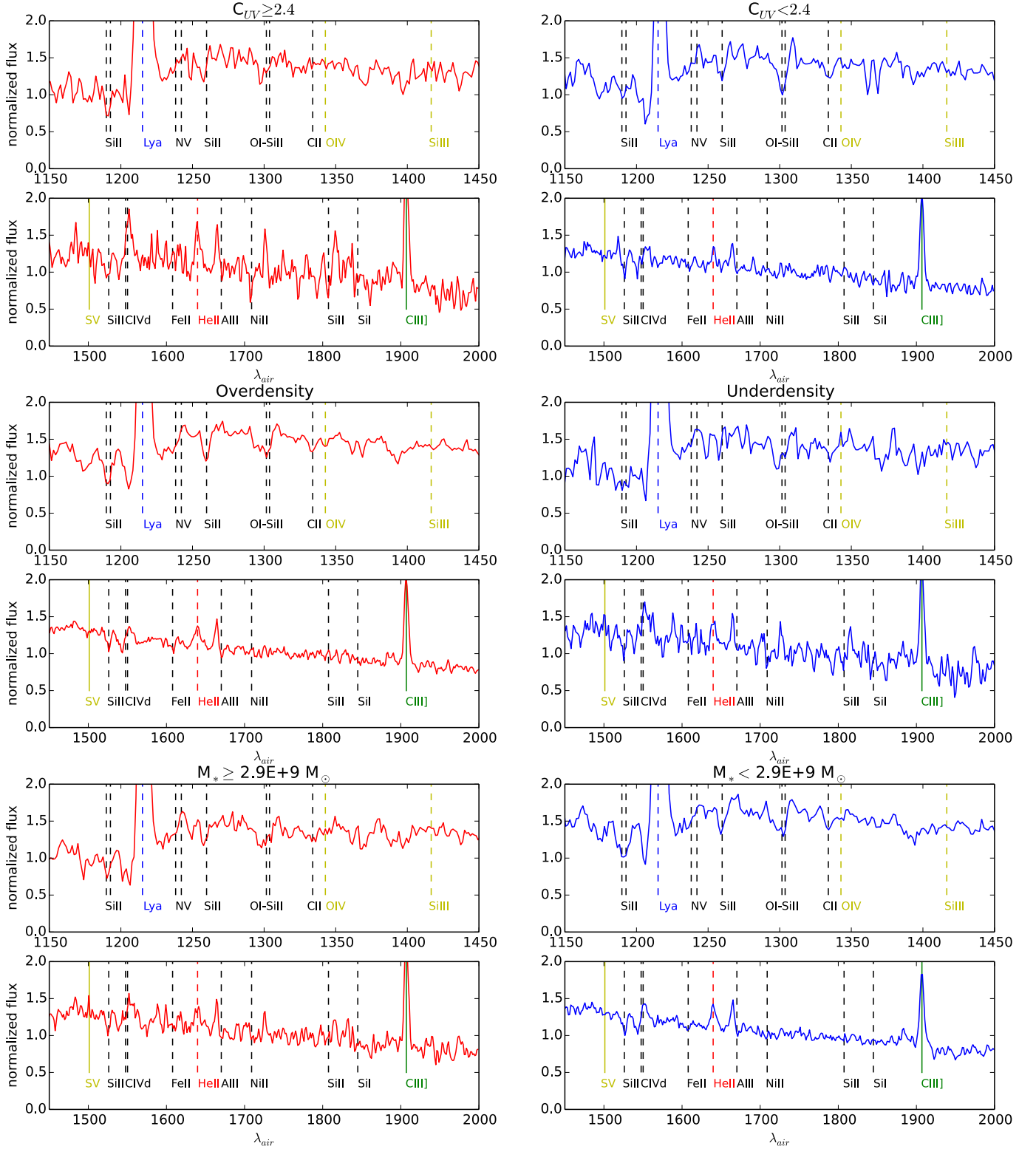
Fig. A.2. Same as Fig. A.1 for the subsamples of the galaxies with $C_{UV} \geq 2.4$, $C_{UV} < 2.4$, located in over- and underdense regions with $M_* \geq 2.9E+9\ M_\odot$, and $M_* < 2.9E+9\ M_\odot$.

Figure A.3 shows a zoom of the stacked spectra on the Lyα wavelength. The Lyα main peak is redshifted with respect to the systemic redshift for all the subsets studied here.
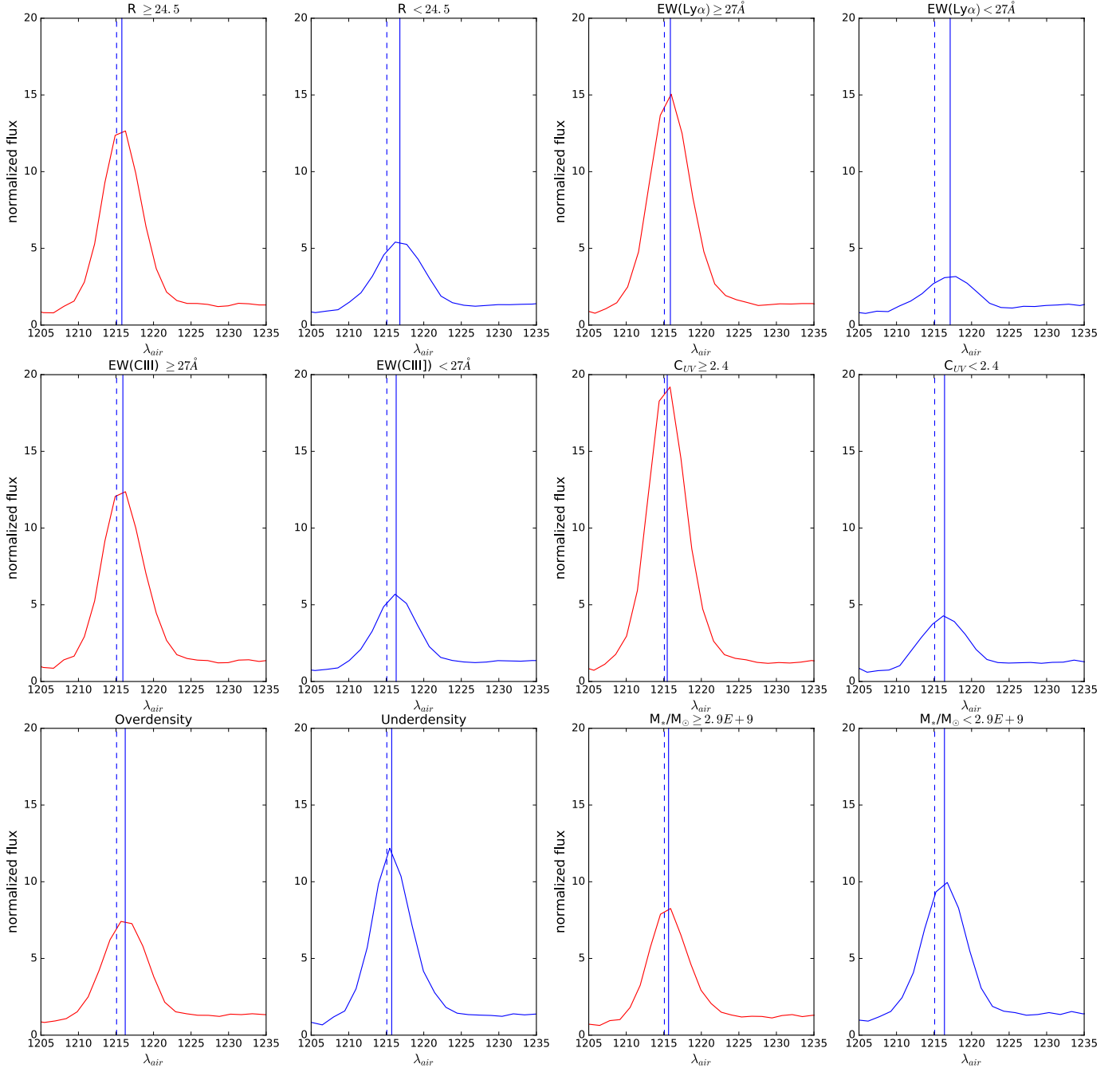
Fig. A.3. Zoom on the Lyα emission line of the stacked spectra in Figs. A.1 and A.2. Vertical dashed lines indicate the rest-frame Lyα wavelength, while the vertical solid lines indicate the wavelength of the red peak.